

---

# Continuous Diffusion for Mixed-Type Tabular Data

---

Markus Mueller

Kathrin Gruber

Dennis Fok

Econometric Institute

Erasmus University Rotterdam

{mueller, gruber, dfok}@ese.eur.nl

## Abstract

Score-based generative models (or diffusion models for short) have proven successful for generating text and image data. However, the adaption of this model family to tabular data of mixed-type has fallen short so far. In this paper, we propose CDTD, a Continuous Diffusion model for mixed-type Tabular Data. Specifically, we combine score matching and score interpolation to ensure a common continuous noise distribution for *both* continuous and categorical features alike. We counteract the high heterogeneity inherent to data of mixed-type with distinct, adaptive noise schedules per feature or per data type. The learnable noise schedules ensure optimally allocated model capacity and balanced generative capability. We homogenize the data types further with model-specific loss calibration and initialization schemes tailored to mixed-type tabular data. Our experimental results show that CDTD consistently outperforms state-of-the-art benchmark models, captures feature correlations exceptionally well, and that heterogeneity in the noise schedule design boosts the sample quality.

## 1 Introduction

Score-based generative models (Song et al., 2021), also termed diffusion models (Sohl-Dickstein et al., 2015; Ho et al., 2020), have shown remarkable potential for the generation of images (Dhariwal & Nichol, 2021; Rombach et al., 2022), videos (Ho et al., 2022), text (Li et al., 2022; Dieleman et al., 2022; Wu et al., 2023), molecules (Hoogeboom et al., 2022), and many other highly complex data structures with continuous features. The framework has since been adapted to categorical data in various ways, including discrete diffusion processes (Austin et al., 2021; Hoogeboom et al., 2021), diffusion in continuous embedding space (Dieleman et al., 2022; Li et al., 2022; Regol & Coates, 2023; Strudel et al., 2022), and others (Campbell et al., 2022; Meng et al., 2022; Sun et al., 2023). Diffusion models which include both, continuous and categorical features alike, build directly on advances from the image domain (Kim et al., 2023; Kotelnikov et al., 2023; Lee et al., 2023; Jolicœur-Martineau et al., 2024) and thus, are not designed to deal with challenges specific to mixed-type data: The different diffusion processes are not aligned, and do not scale to larger datasets and/or features with a greater number of categories.

A crucial component in score-based generative models is the noise schedule (Kingma et al., 2022; Chen et al., 2022; Chen, 2023; Jabri et al., 2022; Wu et al., 2023). Typical noise schedules for image and text data are designed to focus model capacity on the noise levels most important to sample quality (Nichol & Dhariwal, 2021; Karras et al., 2022), while others attempt to learn the optimal noise schedule (Dieleman et al., 2022; Kingma et al., 2022). For mixed-type tabular data, existing approaches often combine distinct diffusion processes for the continuous and discrete features to derive a joint model (Kotelnikov et al., 2023; Lee et al., 2023). However, noise schedules are not directly transferable from one data modality to another and therefore, using specifications from image or text domain models is not optimal: First, the inherently different diffusion processes make it difficult to balance the noise schedules across features and feature types, and negatively affect the

allocation of model capacity across timesteps. Further, and most importantly, the domain, nature and marginal distribution can vary significantly across features (Xu et al., 2019). For instance, any two continuous features may be subject to different levels of discretization or different bounds, even after applying common data pre-processing techniques; and any two categorical features may differ in the number of categories, or the degree of imbalance. This high heterogeneity warrants a rethinking of fundamental parts of the diffusion framework, including the noise schedule and the effective combination of diffusion processes for different data types.

In this paper, we introduce *Continuous Diffusion for mixed-type Tabular Data* (CDTD) to address the aforementioned shortcomings. We combine *score matching* (Hyvärinen, 2005) with *score interpolation* (Dieleman et al., 2022) to derive a score-based model that pushes the diffusion process for categorical data into embedding space, and uses a Gaussian diffusion process for *both* continuous and categorical features. This way, the different noise processes become directly comparable, easier to balance, and enable the application of, for instance, classifier-free guidance (Ho & Salimans, 2022), accelerated sampling (Lu et al., 2022), and other advances, to mixed-type tabular data.

We counteract the high feature heterogeneity inherent to data of mixed-type with distinct feature- or type-specific adaptive noise schedules. The learnable noise schedules allow the model to directly take feature or type heterogeneity into account during both training and generation, and thus avoid the reliance on image or text-specific noise schedules designs. This ensures a better allocation of the model’s capacity across features, feature types and timesteps, and guarantees high quality samples of tabular data. CDTD outperforms state-of-the-art baseline models across a diverse set of sample quality metrics, and computation time for data sets with an arbitrary number of categories and data points. Our experiments show that CDTD captures feature correlations exceptionally well, and that explicitly allowing for data-type heterogeneity in the noise schedules benefits sample quality.

In sum, we make several contributions specific to diffusion probabilistic modeling of tabular data:

- We propose a joint continuous diffusion model for *both* continuous and categorical features such that all noise distributions can be Gaussian.
- We balance model capacity across continuous and categorical features with a novel and effective loss calibration.
- We derive a functional form to learn adaptive noise schedules and to allow for an efficient, exact evaluation and thus, greatly extend the idea of timewarping.
- We drastically improve the scalability of tabular data diffusion models to features with a high number of categories.
- We boost the quality of the generated samples with adaptive, feature- or type-specific noise schedules.
- Our novel combination of score estimation methods allows for the application of state-of-the-art techniques, such as classifier-free guidance and accelerated sampling, to mixed-type tabular data for the first time.

## 2 Score-based Generative Framework

We start with a brief outline of the score-based frameworks for continuous and categorical features. Next, we combine these into a single diffusion model to learn the joint distribution of mixed-type data.

### 2.1 Continuous Features

We denote the  $i$ -th continuous feature as  $x_{\text{cont}}^{(i)} \in \mathbb{R}$  and the stacked feature vector as  $\mathbf{x}_0 \equiv \mathbf{x}_{\text{cont}} \in \mathbb{R}^{K_{\text{cont}}}$ . Further, let  $\{\mathbf{x}_t\}_{t=0}^1$  be a diffusion process that gradually adds noise in continuous time  $t \in [0, 1]$  to  $\mathbf{x}_0$ , and let  $p_t(\mathbf{x})$  denote the density function of the data at time  $t$ . Then, this process transforms the real data distribution  $p_0(\mathbf{x})$  into a terminal distribution of pure noise  $p_1(\mathbf{x})$  from which we can sample. Our goal is to learn the reverse process that allows us to go from noise  $\mathbf{x}_1 \sim p_1(\mathbf{x})$  to a new data sample  $\mathbf{x}_0^* \sim p_0(\mathbf{x})$ .

The forward-pass of this continuous-time diffusion process is formulated as the solution to a stochastic differential equation (SDE):

$$d\mathbf{x} = \mathbf{f}(\mathbf{x}, t)dt + g(t)d\mathbf{w}, \tag{1}$$

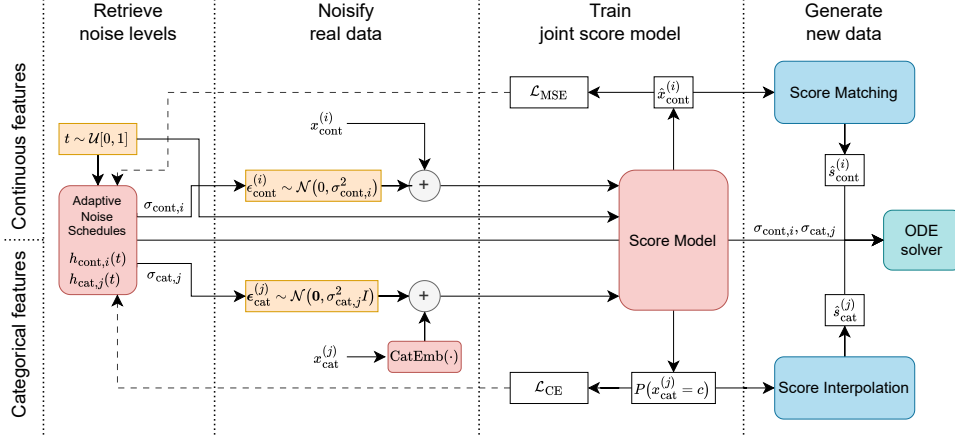


Figure 1: CDTD framework. Adaptive noise schedules are trained to fit the (possibly aggregated) MSE and CE losses and transform the uniform timestep  $t$  to a potentially feature-specific noise level to diffuse (“noisify”) the scalar values (for continuous features) or the embeddings (for categorical features). Associated sampling processes are highlighted in orange. The approximated score functions are concatenated and passed to a blackbox ODE solver for sample generation.

where  $\mathbf{f}(\cdot, t) : \mathbb{R}^{K_{\text{cont}}} \rightarrow \mathbb{R}^{K_{\text{cont}}}$  is the drift coefficient,  $g(\cdot) : \mathbb{R} \rightarrow \mathbb{R}$  is the diffusion coefficient, and  $\mathbf{w}$  is a Brownian motion (Song et al., 2021). The reversion yields the trajectory of  $\mathbf{x}$  as  $t$  goes backwards in time from 1 to 0, and is formulated as a probability flow ordinary differential equation (ODE):

$$d\mathbf{x} = \left[ \mathbf{f}(\mathbf{x}, t) - \frac{1}{2}g(t)^2 \nabla_{\mathbf{x}} \log p_t(\mathbf{x}) \right] dt. \quad (2)$$

We approximate the score function  $\nabla_{\mathbf{x}} \log p_t(\mathbf{x})$ , the only unknown in Equation (2), by training a time-dependent score-based model  $s_{\theta}(\mathbf{x}, t)$  via *score matching* (Hyvärinen, 2005). The parameters  $\theta$  are trained to minimize the *denoising score matching* objective:

$$\mathbb{E}_t \left[ \lambda_t \mathbb{E}_{\mathbf{x}_0} \mathbb{E}_{\mathbf{x}_t | \mathbf{x}_0} \left\| s_{\theta}(\mathbf{x}_t, t) - \nabla_{\mathbf{x}_t} \log p_{0t}(\mathbf{x}_t | \mathbf{x}_0) \right\|_2^2 \right], \quad (3)$$

where  $\lambda_t : [0, 1] \rightarrow \mathbb{R}_+$  is a positive weighting function for timesteps  $t \sim \mathcal{U}_{[0,1]}$ , and  $p_{0t}(\mathbf{x}_t | \mathbf{x}_0)$  is the density of the noisy  $\mathbf{x}_t$  given the ground-truth data  $\mathbf{x}_0$  (Vincent, 2011).

In this paper, we use the EDM formulation (Karras et al., 2022), that is,  $\mathbf{f}(\cdot, t) = \mathbf{0}$  and  $g(t) = \sqrt{2 \left[ \frac{d}{dt} \sigma(t) \right] \sigma(t)}$  such that  $p_{0t}(\mathbf{x}_t | \mathbf{x}_0) = \mathcal{N}(\mathbf{x}_t | \mathbf{x}_0, \sigma^2(t) I_{K_{\text{cont}}})$ . We start the reverse process with sampling  $\mathbf{x}_1 \sim p_1(\mathbf{x}) = \mathcal{N}(\mathbf{0}, \sigma^2(1) I_{K_{\text{cont}}})$  for  $\sigma^2(1)$  being sufficiently large and  $\mathbb{E}[\mathbf{x}_0] = \mathbf{0}$ . We then gradually guide  $\mathbf{x}_1$  towards high density regions in the data space with  $s_{\theta}(\mathbf{x}, t)$  replacing the unknown, true score function in Equation (2). In practice, ODE or predictor-corrector samplers can be used for this iterative denoising process (Song et al., 2021).

## 2.2 Categorical Features

For categorical features, the score function is undefined and the score-based generative framework cannot be directly applied. Therefore, we use *score interpolation* (Dieleman et al., 2022) and push the diffusion of categorical data into Euclidean embedding space. This allows us to impose a Gaussian noise distribution on categorical *and* continuous features.

Let  $x_{\text{cat}}^{(j)} \in \{1, \dots, C_j\}$  be the  $j$ -th categorical feature with  $C_j$  possible classes. The  $i$ -th class is associated to a distinct, trainable  $d$ -dimensional embedding vector  $\mathbf{e}_i^{(j)} \in \mathbb{R}^d$ . The embedding vector corresponding to the ground truth class is  $\mathbf{x}_0^{(j)} \in \{\mathbf{e}_1^{(j)}, \dots, \mathbf{e}_{C_j}^{(j)}\}$ . We omit the superscript  $j$  in what follows. The noisy variant at time  $t$  is  $\mathbf{x}_t \sim p_{0t}(\mathbf{x}_t | \mathbf{x}_0) = \mathcal{N}(\mathbf{x}_t | \mathbf{x}_0, \sigma^2(t) I_d)$  similar to before. Given  $\mathbf{x}_t$  and  $t$ ,  $\mathbb{E}_{p(\mathbf{x}_0 | \mathbf{x}_t, t)} [\nabla_{\mathbf{x}_t} \log p_{0t}(\mathbf{x}_t | \mathbf{x}_0)]$  minimizes Equation (3), and we obtain

$$\mathbb{E}_{p(\mathbf{x}_0 | \mathbf{x}_t, t)} \nabla_{\mathbf{x}_t} \log p_{0t}(\mathbf{x}_t | \mathbf{x}_0) = \frac{1}{\sigma_t^2} \left[ \mathbb{E}_{p(\mathbf{x}_0 | \mathbf{x}_t, t)} [\mathbf{x}_0] - \mathbf{x}_t \right]. \quad (4)$$

We compute  $\hat{\mathbf{x}}_0 = \mathbb{E}_{p(\mathbf{x}_0|\mathbf{x}_t, t)}[\mathbf{x}_0]$  as an average over the  $C_j$  possible embedding vectors weighted by their probability. This yields a score function estimate for a single categorical feature. Since  $p(\mathbf{x}_0 = \mathbf{e}_i|\mathbf{x}_t, t) = p(x_{\text{cat}}^{(j)} = i|\mathbf{x}_t, t)$ , an estimate of  $p(\mathbf{x}_0|\mathbf{x}_t, t)$  is obtained via a classifier that predicts  $C_j$  class probabilities for the  $j$ -th feature and is trained via cross-entropy (CE) loss.

Likewise, we start the generative process for a categorical feature from an embedding vector  $\mathbf{x}_1 \sim p_1(\mathbf{x}) = \mathcal{N}(\mathbf{0}, \sigma^2(1)I_d)$ . We then use score interpolation to iteratively denoise the embedding vector. After the last timestep in the reverse process, that is,  $t \approx 0$ , we directly infer the generated class from the feature-specific class probabilities,  $p(\mathbf{x}_0 = \mathbf{e}_i|\mathbf{x}_t, t)$ .

This framework can easily be extended to multiple categorical features. All embeddings are trained alongside the model. The model fully takes feature-specific uncertainty at intermediate timesteps into account (for each feature it only has to commit to a category at the final step of generation) which improves the consistency of the generated samples (Dieleman et al., 2022). Therefore, CDTD allows to capture subtle dependencies both *within* and *across* data types more accurately.

### 3 Method

In short, we combine *score matching* (Equation (3)) with *score interpolation* (Equation (4)) to model the joint distribution of mixed-type data. Next, we discuss the important components of our method. In particular, the combination of the different losses for score interpolation and score matching, initialization and loss weighting concerns, and the adaptive type- or feature-specific noise schedule designs.

#### 3.1 General Framework

Figure 1 gives an overview of our Continuous Diffusion for mixed-type Tabular Data (CDTD) framework. The score model is conditioned on (1) all noisy continuous features, (2) the noisy embeddings of all categorical features in Euclidean space, and (3) the timestep  $t$  which reflects potentially feature-specific, adaptive noise levels  $\sigma_{\text{cont}, i}$  and  $\sigma_{\text{cat}, j}$  for all  $i$  and  $j$ . Additional conditioning information, such as the target feature for classification tasks, are straightforward to add. Note that while the Gaussian noise process acts directly on the continuous features, it acts on the embeddings of the categorical features. This way, we ensure a common continuous noise process for both data types.

During training, the model predicts the ground-truth value for continuous features and the class-specific probabilities for categorical features. During generation, we concatenate the score estimates,  $\hat{s}_{\text{cont}}^{(i)}$  and  $\hat{s}_{\text{cat}}^{(j)}$ , for all features  $i$  and  $j$ , and pass them to an ODE solver together with  $\sigma_{\text{cont}, i}$  and  $\sigma_{\text{cat}, j}$ , the noise levels retrieved by transforming linearly spaced timesteps with the learned adaptive noise schedules. Further implementation details are provided in Appendix J.

#### 3.2 Homogenization of Data Types

Let  $\mathcal{L}_{\text{MSE}}(x_{\text{cont}}^{(i)}, t)$  denote the time-weighted MSE (i.e., score matching in Equation (3)) loss of the  $i$ -th continuous feature at a single timestep  $t$ , and  $\mathcal{L}_{\text{CE}}(x_{\text{cat}}^{(j)}, t)$  the CE (i.e. score interpolation) loss of the  $j$ -th categorical feature. Naturally, the two losses are defined on different scales. This leads to an unintended importance weighting of features in the generative process. We assume that an unconditional model should a priori, i.e., without having any information, be indifferent between all features. This reflects the state of the model at the terminal timestep  $t = 1$  in the diffusion process.

Formally, we aim to find calibrated losses,  $\mathcal{L}_{\text{MSE}}^*$  and  $\mathcal{L}_{\text{CE}}^*$  for all continuous features  $i$  and categorical features  $j$ , such that

$$\mathbb{E}[\mathcal{L}_{\text{MSE}}^*(x_{\text{cont}}^{(i)}, 1)] = \mathbb{E}[\mathcal{L}_{\text{CE}}^*(x_{\text{cat}}^{(j)}, 1)] = 1. \quad (5)$$

For continuous features,  $\mathbb{E}[\mathcal{L}_{\text{MSE}}^*(x_{\text{cont}}^{(i)}, 1)] = 1$  follows from standardizing  $x_{\text{cont}}^{(i)}$  to zero mean and unit variance. For categorical features, we compute the normalization constant  $\mathbb{E}[\mathcal{L}_{\text{CE}}(x_{\text{cat}}^{(j)}, 1)]$  directly as the CE of each predicted class in proportion to its empirical distribution in the train set (see Appendix A). We then average the calibrated losses to derive the joint loss function at a given timestep:

$$\mathcal{L}(t) = \frac{1}{K} \left[ \sum_{i=1}^{K_{\text{cont}}} \mathcal{L}_{\text{MSE}}^*(x_{\text{cont}}^{(i)}, t) + \sum_{j=1}^{K_{\text{cat}}} \mathcal{L}_{\text{CE}}^*(x_{\text{cat}}^{(j)}, t) \right], \quad (6)$$

where  $K = K_{\text{cont}} + K_{\text{cat}}$ .

The loss calibration and the multiple data modalities have implications for the optimal initialization of the score model. We aim to initialize all *feature-specific* losses at one. We therefore initialize the output layer weights to zero (like in image diffusion models) and the output biases for continuous features to zero, and rely on the timestep weights of the EDM parameterization (Karras et al., 2022) to achieve a unit loss for all  $t$ . For the categorical features, we initialize the biases to match the category’s empirical probability in the training set (see Appendix B).

The initial equal importance across all timesteps will naturally change over the course of training. We employ an normalization scheme for the average diffusion loss (Karras et al., 2023; Kingma & Gao, 2023) to allow for changes in relative importance among features but ensure equal importance of all timesteps throughout training. To do so, we learn the time-specific normalization term  $Z(t)$  such that  $\mathcal{L}(t)/Z(t) \approx 1$ . This ensures a consistent gradient signal and can be implemented by training a neural network to predict  $\mathcal{L}(t)$  alongside our diffusion model (for details see Appendix C).

### 3.3 Noise Schedules

Since the optimal noise schedule of one feature impacts the noise schedules of other features, and the different data types have different sensitivities to additive noise, we introduce *feature-specific* or *type-specific* noise schedules. For instance, given the same embedding dimension, more noise is needed to remove the same amount of signal from embeddings of features with fewer classes. Likewise, a delayed noise schedule for one feature might improve sample quality as the model can rely on other correlated features that have been (partially) generated first. We make the noise schedules learnable, and therewith *adaptive* to avoid the reliance on designs for other data modalities.

We investigate the following noise schedule variants: (1) a single adaptive noise schedule, (2) adaptive noise schedules differentiated per data type and (3) feature-specific adaptive noise schedules. We only introduce the feature-specific noise schedules explicitly. The other noise schedule types are easily derived from our argument by appropriately aggregating terms across features.

**Feature-specific Noise Schedules.** According to Equation (1), and following the EDM parameterization (Karras et al., 2022), we define the diffusion process of the  $i$ -th continuous feature as

$$dx_{\text{cont}}^{(i)} = \sqrt{2 \left[ \frac{d}{dt} h_{\text{cont},i}(t) \right] h_{\text{cont},i}(t) dw_t^{(i)}}, \quad (7)$$

and likewise the trajectory of the  $j$ -th categorical feature as

$$dx_{\text{cat}}^{(j)} = \sqrt{2 \left[ \frac{d}{dt} h_{\text{cat},j}(t) \right] h_{\text{cat},j}(t) d\mathbf{w}_t^{(j)}}, \quad (8)$$

where  $\mathbf{x}_{\text{cat}}^{(j)}$  is the  $d$ -dimensional embedding of  $x_{\text{cat}}^{(j)}$  in Euclidean space. The *feature-specific* noise schedules  $h_{\text{cont},i}(t)$  and  $h_{\text{cat},j}(t)$  represent the standard deviations of the added Gaussian noise such that  $\sigma_{\text{cont},i}(t) = h_{\text{cont},i}(t)$  and  $\sigma_{\text{cat},j}(t) = h_{\text{cat},j}(t)$ . Thus, each continuous feature and each embedded categorical feature is affected by a distinct noise schedule.

**Adaptive Noise Schedules.** We aim to learn a noise schedule  $h_k : t \mapsto \sigma$  for all  $K = K_{\text{cont}} + K_{\text{cat}}$  features. Note that  $t \in [0, 1]$ , and with pre-specified minimum and maximum noise levels, we can scale  $\sigma_k$  to lie in  $[0, 1]$  as well, without loss of generality. We will learn the feature-specific loss given the noise level,  $F_k : \sigma_k \mapsto \ell_k$ , alongside the score model, with  $\ell_k$  the relevant (not explicitly weighted) training loss for the  $k$ -th feature. Then, our mapping of interest is  $h_k = \tilde{F}_k^{-1}$ , that is, the normalized and inverted function  $F_k$ . This encourages the relation between  $t$  and  $\ell_k$  to be linear.

Higher noise levels imply a lower signal-to-noise ratio, and therefore a larger incurred loss for the score model. Accordingly,  $F_k$  must be a monotonically increasing and *S-shaped* function. We let  $F_k = \gamma_k F_{\text{d.a.log},k}(\sigma_k)$  where  $\gamma_k > 0$  is a scaling factor that at  $t = 1$  enables fitting a loss  $\ell_k > 1$  early on in the training process, and a loss  $\ell_k < 1$  in case conditioning information is included. Further, we use the cdf of the domain-adapted Logistic distribution  $F_{\text{d.a.log},k}(\sigma_k)$ , where the input is pre-processed via a Logit function, with parameters  $0 < \mu_k < 1$  (the location of the inflection point) and  $\nu_k \geq 1$  (the steepness of the curve). Figure 2 illustrates the effect of the location parameter. The implicit importance of the noise levels is conveniently represented by the corresponding pdf  $f_{\text{d.a.log},k}$ .

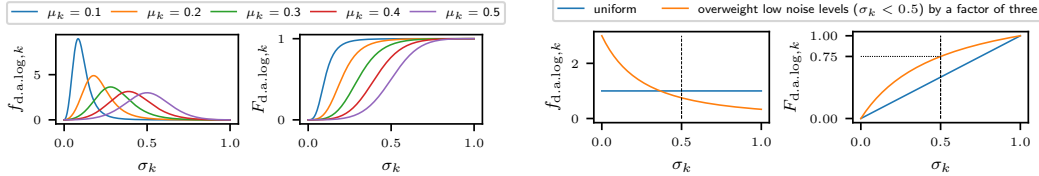


Figure 2: (Left) pdf ( $f_{d.a.log,k}$ ) and cdf ( $F_{d.a.log,k}$ ) of the domain-adapted Logistic distribution for five different values of the location parameter  $\mu_k$  and for a given curve steepness  $\nu_k = 3$ . (Right) impact of uniform vs. adjusted timewarping initialization on the pdf ( $f_{d.a.log,k}$ ) and the cdf ( $F_{d.a.log,k}$ ).

To normalize and invert  $F_k$ , we set  $\gamma_k = 1$  and directly utilize the quantile function  $F_{d.a.log,k}^{-1}$ . The detailed derivation of all relevant functions is given in Appendix D.

Our functional choice has several advantages. First, each noise schedule can be evaluated exactly without the need for approximations and only requires three parameters. Second, these parameters are well interpretable in the diffusion context and provide information on the inner workings of the model. For instance, for  $\mu_1 < \mu_2$ , the model starts generating feature 2 before feature 1 in the reverse process. Third, the proposed functional form is less flexible than the original piece-wise linear function (Dieleman et al., 2022) such that an exponential moving average on the parameters is not necessary, and the fit is more robust to ‘‘outliers’’ encountered during training.

We use the adaptive noise schedules during both training and generation. We derive importance weights from  $f_{d.a.log,k}$  to fit  $h_k$  to avoid biasing the noise schedule to timesteps that are frequently sampled during training. Type-specific noise schedules refer to learning two functions  $F_1$  and  $F_2$  that predict the respective average loss over all features of a data type. Examples of learned noise schedules are given in Appendix K.

### 3.4 Additional Customization to Tabular Data

In the diffusion process, we add noise directly to the continuous features but to the embeddings of categorical features. We generally need more noise to remove all signal from the categorical representations. We therefore define *type-specific* minimum and maximum noise levels: For categorical features, we let  $\sigma_{cat,min} = 0.1$  and  $\sigma_{cat,max} = 100$ ; for continuous features, we set  $\sigma_{cont,min} = 0.002$  and  $\sigma_{cont,max} = 80$  (see Karras et al., 2022).

Lastly, an uninformative initialization of the adaptive noise schedules requires to set  $\mu_k = 0.5$ ,  $\nu_k \approx 1$  and  $\gamma_k = 1$  such that  $F_{d.a.log,k}$  corresponds approximately to the cdf of a uniform distribution. We can improve this with a more informative prior: In the image domain, diffusion models allocate substantial capacity towards generating the high level structure before generating details at lower noise levels. In tabular data, the location of features in the data matrix, and therefore the high level structure, is fixed. Instead, we are interested in generating details as accurately as possible, as these influence, for instance, subtle correlations among features. Note that the inflection point,  $\mu_k$ , of our adaptive noise schedule corresponds to the proportion of high (normalized) noise levels (i.e.,  $\sigma_k \geq 0.5$ ) in the distribution. Therefore, we adjust the initial noise schedules such that low noise levels ( $\sigma_k < 0.5$ ) are weighted by a factor of 3 relative to high noise levels ( $\sigma_k \geq 0.5$ ) (see Figure 2). The proportion of high noise levels is decreased to  $\mu_k = 1/4$ . We let  $\nu_k \approx 1$  for a dispersed initial probability mass and initialize the scaling factor to  $\gamma_k = 1$ .

## 4 Experiments

We benchmark our model against several generative models across multiple datasets. Additionally, we investigate three different noise schedule specifications: (1) a single adaptive noise schedule for both data types (*single*), (2) continuous and categorical data type-specific adaptive noise schedules (*per type*), and (3) feature-specific adaptive noise schedules (*per feature*).

**Baseline models.** We use a diverse benchmark set of state-of-the-art generative models for mixed-type tabular data. This includes ARF (Watson et al., 2023), CTGAN (Xu et al., 2019), TVAE (Xu et al., 2019), TabDDPM (Kotelnikov et al., 2023), and CoDi (Lee et al., 2023). Each model follows a different design and/or modeling philosophy. Note that CoDi is an extension of STaSy (Kim et al., 2023, the same group of authors) that has shown to be superior in performance. For scaling

reasons, the recently proposed Diffusion Forest (Jolicoeur-Martineau et al., 2024) is not an applicable benchmark. Further details on the respective benchmark models and their implementations are provided in Appendix F and Appendix G. To keep the comparison fair, we use the same architecture for CDTD as TabDDPM, with minor changes to accommodate the different inputs (see Appendix J).

**Datasets.** We systematically investigate our model on eleven publicly available datasets. The datasets vary in size, prediction task (regression vs. binary classification), number of continuous *and* categorical features and their distributions. The number of categories for categorical features varies significantly across datasets (for more details, see Appendix E). We remove observations with missings in the target or any of the continuous features and encode missings in the categorical features as a separate category. All datasets are split in train (60%), validation (20%) and test (20%) partitions, hereinafter denoted  $\mathcal{D}_{\text{train}}$ ,  $\mathcal{D}_{\text{valid}}$  and  $\mathcal{D}_{\text{test}}$ , respectively. For classification tasks, we use stratification with respect to the outcome, we condition the model on the outcome during training and generation, and use the train set proportions for generation. In a last post-processing step, we round the integer-valued continuous features after generation for all models.

#### 4.1 Evaluation Metrics

We evaluate all generative models on four sample quality criteria after generating synthetic data  $\mathcal{D}_{\text{gen}}$  of size  $\min(|\mathcal{D}_{\text{train}}|, 50\,000)$ . All metrics are averaged over five random seeds that affect the generative process.

**Machine learning efficiency.** We follow the conventional train-synthetic-test-real strategy (see, Borisov et al., 2023; Liu et al., 2023; Kotelnikov et al., 2023; Kim et al., 2023; Xu et al., 2019; Watson et al., 2023). Hence, we train a group of models, consisting of a (logistic/ridge) regression, a random forest and a catboost model, on the data-specific prediction task (the corresponding hyperparameter settings are reported in Appendix I). We compare the model-averaged real test performance,  $\text{Perf}(\mathcal{D}_{\text{train}}, \mathcal{D}_{\text{test}})$ , to the performance trained on the synthetic data,  $\text{Perf}(\mathcal{D}_{\text{gen}}, \mathcal{D}_{\text{test}})$ . We subsample  $\mathcal{D}_{\text{train}}$  in case of more than 50 000 observations to upper-bound the computational load. The results are averaged over ten different model seeds (in addition to the five random seeds that impact the sampling process). For regression tasks, we consider the RMSE and for classification tasks, the macro-averaged F1 and AUC scores. We only report  $|\text{Perf}(\mathcal{D}_{\text{gen}}, \mathcal{D}_{\text{test}}) - \text{Perf}(\mathcal{D}_{\text{train}}, \mathcal{D}_{\text{test}})|$  in the main part of this paper. An absolute difference close to zero, that is, synthetic and real data induce the same performance, indicates that the generative model performs well.

**Detection score.** For each generative model, we report the accuracy of a catboost model that is trained to distinguish between real and generated (fake) samples (Borisov et al., 2023; Liu et al., 2023). First, we subsample the real data subsets,  $\mathcal{D}_{\text{train}}$ ,  $\mathcal{D}_{\text{valid}}$  and  $\mathcal{D}_{\text{test}}$ , to a maximum of 25 000 data samples to limit evaluation time. Then, we construct  $\mathcal{D}_{\text{train}}^{\text{detect}}$ ,  $\mathcal{D}_{\text{valid}}^{\text{detect}}$  and  $\mathcal{D}_{\text{test}}^{\text{detect}}$  with equal proportions of real and fake samples. We tune each catboost model on  $\mathcal{D}_{\text{valid}}^{\text{detect}}$  and report the accuracy of the best-fitting model on  $\mathcal{D}_{\text{test}}^{\text{detect}}$  (see Appendix H for details). A (perfect) detection score of 0.5 indicates the model is unable distinguish fake from real samples.

**Statistical similarity.** We evaluate the statistical similarity between real and generated training data based on: (1) the Jensen-Shannon divergence (JSD; Lin, 1991) to quantify the difference in categorical distributions, (2) the Wasserstein distance (WD; Ramdas et al., 2017) to quantify the difference in continuous distributions, and (3) the  $L_2$  distance of the pair-wise correlation matrices. We use the Pearson correlation coefficient for the correlations between two continuous features, the Theil uncertainty coefficient for the correlations between two categorical features, and the correlation ratio across types (Kotelnikov et al., 2023; Zhao et al., 2021).

**Distance to closest record.** That is, the minimum Euclidean distance of a generated data point to any observation in  $\mathcal{D}_{\text{train}}$  (Borisov et al., 2023; Zhao et al., 2021). We one-hot encode categorical features and standardize all features to zero mean and unit variance to ensure each feature contributes equally to the distance. We compute the average distance to closest record (DCR) as a robust estimate. For brevity, we report the absolute difference of the DCR of the synthetic data and the DCR of the real test set. A good DCR value, that indicates realistic and sufficiently private data, should be close to zero.

Table 1: Average performance rank of each generative model across eleven datasets. Per performance metric, **bold** indicates the best, underline the second best result. CoDi is prohibitively expensive to train on `lending` and `diabetes`, TabDDPM produces NaNs for `acsincome` and `diabetes`, and therefore get assigned rank 8 for these datasets.

	ARF	CTGAN	TVAE	TabDDPM	CoDi	CTD (single)	CTD (per type)	CTD (per feature)
RMSE	3.000 $\pm$ 1.673	6.400 $\pm$ 1.356	6.200 $\pm$ 1.833	6.400 $\pm$ 1.200	5.600 $\pm$ 1.356	<b>2.400</b> $\pm$ 0.490	<u>2.600</u> $\pm$ 1.855	3.400 $\pm$ 2.059
F1	5.167 $\pm$ 1.951	6.667 $\pm$ 1.374	6.667 $\pm$ 0.745	<u>3.333</u> $\pm$ 2.285	5.333 $\pm$ 2.494	<u>3.333</u> $\pm$ 1.247	<b>2.667</b> $\pm$ 1.106	3.000 $\pm$ 1.915
AUC	4.500 $\pm$ 1.607	7.000 $\pm$ 1.155	6.500 $\pm$ 0.764	4.167 $\pm$ 2.115	6.000 $\pm$ 2.160	<u>2.333</u> $\pm$ 1.599	<b>2.167</b> $\pm$ 0.898	3.500 $\pm$ 1.500
L <sub>2</sub> dist. of corr.	4.455 $\pm$ 1.305	6.727 $\pm$ 1.213	6.455 $\pm$ 1.157	5.636 $\pm$ 2.346	5.545 $\pm$ 1.876	<u>2.545</u> $\pm$ 1.305	<b>2.091</b> $\pm$ 0.793	2.636 $\pm$ 1.553
Detection score	4.818 $\pm$ 1.336	7.182 $\pm$ 1.113	5.636 $\pm$ 0.881	4.000 $\pm$ 2.412	6.459 $\pm$ 1.777	3.273 $\pm$ 0.862	<b>1.818</b> $\pm$ 1.696	<u>2.909</u> $\pm$ 1.505
JSD	<b>1.273</b> $\pm$ 0.617	6.818 $\pm$ 1.113	7.182 $\pm$ 0.716	5.818 $\pm$ 1.641	5.909 $\pm$ 1.083	<u>2.364</u> $\pm$ 0.979	3.000 $\pm$ 0.603	3.727 $\pm$ 1.052
WD	4.273 $\pm$ 1.483	6.000 $\pm$ 1.758	6.455 $\pm$ 1.157	5.000 $\pm$ 2.449	6.727 $\pm$ 1.286	3.000 $\pm$ 1.348	<b>2.273</b> $\pm$ 1.052	<u>2.364</u> $\pm$ 1.494
DCR	4.909 $\pm$ 1.564	6.818 $\pm$ 1.466	5.182 $\pm$ 2.443	3.636 $\pm$ 2.837	5.364 $\pm$ 1.920	3.727 $\pm$ 2.049	<u>3.364</u> $\pm$ 1.611	<b>3.091</b> $\pm$ 1.443

## 4.2 Results

Table 1 shows the ranks of all generative averaged across all datasets for all considered metrics. The ranks in terms of the F1 and AUC scores are averaged over the classification task datasets. Likewise, the RMSE rank averages include the regression task datasets only. We assign the maximum possible rank when a model was not trainable on a given dataset. This includes TabDDPM, which outputs NaNs for `acsincome` and `diabetes` and CoDi, which we consider to be prohibitively expensive to train on `diabetes` (estimated 14.5 hours) and `lending` (estimated 60 hours). The dataset-specific results (including standard errors) and average metrics over all datasets are detailed in Appendix N. We provide visualizations of the captured correlations in the synthetic sample compared to the real training set in Appendix M and distribution plots for a qualitative comparison in Appendix L.

**Sample quality.** CDTD consistently outperforms the considered benchmark models in most sample quality metrics. We see a major performance edge in terms of the detection score, the L<sub>2</sub> distance of the correlation matrices and the regression-based metrics. Only for the Jensen-Shannon divergence, CDTD is dominated by ARF, a tree-based method that is expected to model categorical features particularly well. Interestingly, CDTD performs similar to TabDDPM on F1 scores but outperforms it dramatically for regression tasks. TabDDPM appears to favor modeling categorical features accurately, thereby sacrificing continuous features, as visualized in Appendix M. By utilizing score interpolation, CDTD is able to model intricate correlation structure more accurate than other (multinomial diffusion-based) frameworks. Most importantly, type-specific noise schedules always outperform the feature-specific noise schedule variant and often also the single noise schedule version. This illustrates the importance of accounting for the high heterogeneity in tabular data on the feature type level. Imposing different noise schedules per feature, however, appears to force too many constraints on the model and hence decreases sample quality. Per-feature noise schedules would require more training steps to converge, as can be seen in Appendix K.

**Training and sampling time.** Figure 3 shows the average wall-clock time over all datasets (for which training was feasible for all models) for training as well as the time for sampling 1000 data points of each baseline model and the most complex CDTD variant. Details are given in Appendix P. The use of embeddings (instead of one-hot encoding) for categorical features drastically reduces the training time. CDTD trains the fastest on average and is able to reach a maximum training time of less than 30 min across all datasets. Thus, CDTD exhibits improved scaling to an increase in the number of categories. The ODE definition of the diffusion process also implies competitive sampling speeds compared to TVAE and CTGAN and in particular, to the diffusion-based benchmarks CoDi and TabDDPM. In light of the vastly improved scalability, the CDTD results in Table 1 could in practice trivially be improved further by simply scaling up the architecture.

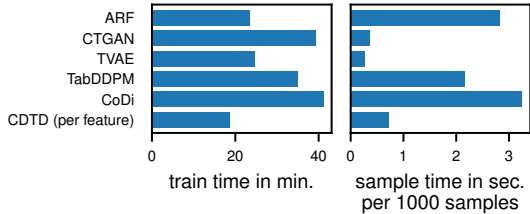


Figure 3: Average wall-clock time for training and for sampling 1000 samples (excluding `acsincome`, `diabetes` and `lending`).



Table 2: Ablation study for five CDTD configurations with progressive addition of model components. We report the median performance metrics over `acsincome`, `adult`, `beijing` and `churn`.

Config.	A	B	C	D	CDTD (per type)
RMSE (abs. diff.; ↓)	0.041	0.042	0.043	0.037	0.033
F1 (abs. diff.; ↓)	0.012	0.013	0.012	0.016	0.015
AUC (abs. diff.; ↓)	0.004	0.005	0.005	0.004	0.004
L <sub>2</sub> distance of corr. (↓)	0.131	0.124	0.146	0.118	0.127
Detection score (↓)	0.577	0.583	0.590	0.561	0.560
JSD (↓)	0.011	0.011	0.011	0.012	0.013
WD (↓)	0.004	0.005	0.005	0.003	0.003
DCR (abs. diff. to test; ↓)	0.405	0.361	0.386	0.299	0.372

**Ablation study.** We conduct an ablation study over four datasets to investigate the separate components of our CDTD framework. The results are given in Table 2 (detailed results are in Appendix O). The baseline model *Config. A* includes a single noise schedule with the original piece-wise linear formulation (Dieleman et al., 2022) without loss normalization, improved model initialization or adaptive normalization, and the CE and MSE losses are naively averaged. Note that this configuration still is a novel contribution to the literature. *Config. B* adds our feature homogenization (i.e., loss normalization, improved initialization and adaptive normalization schemes), *Config. C* adds our proposed functional form for a single noise schedule with uniform initialization, and *Config. D* imposes per-type noise schedules. Lastly, we add the suggested (low noise level) overweighting timewarping initialization to arrive at the full CDTD (*per type*) model. We see the switch from the piece-wise linear functional form to our more robust noise schedule variant slightly harms sample quality. However, the per-type variant and the more informed initialization scheme compensate for this difference. Main differences are in the RMSE and detection score as well as training efficiency (the loss calibration and improved initialization facilitate model convergence). The final model especially works well on the larger datasets compared to the baseline (see Appendix O), as smaller datasets are relatively easy to fit with 3 million parameters, even without any model improvements.

## 5 Conclusion and Discussion

We propose a Continuous Diffusion model for mixed-type Tabular Data (CDTD) that combines score matching and score interpolation and imposes Gaussian diffusion processes on both continuous and embedded categorical features. We compared to various benchmark models and to a single noise schedule as typically used in image diffusion models. Our results indicate that acknowledging the high feature heterogeneity in tabular data on the feature type level and aligning type-specific diffusion elements, such as the noise schedules or losses, substantially benefits sample quality. CDTD also shows vastly improved scalability and can accommodate an arbitrary number of categories.

Our paper serves as an important step to adopting the diffusion probabilistic framework customized to tabular data. In particular, the common type of noise schedules allows for a framework that is easy to extend and may accelerate progress on diffusion models for tabular data. Crucially, CDTD allows the direct application of diffusion-related advances from the image domain, like classifier-free guidance, to tabular data. We leave further extensions, e.g., the exploration of accelerated sampling, efficient score model architectures, or different forms of adaptive noise schedules, to future work.

Finally, we want to highlight that synthetic data could be misused to support unwarranted claims. In any case, any generated data should not be blindly trusted and synthetic data based inferences should be compared to results derived from the real data. On the other hand, the correct usage of generative models can allow for better privacy preservation, facilitate data sharing and open science practices.

## Limitations

The main limitation of the CDTD model is the addition of another hyperparameter, i.e., the type of noise schedule, and tuning a hyperparameter of a generative model can be a costly endeavor. However, our results also show that a per type schedule is most often optimal. Dieleman et al. (2022) show that the results of score interpolation can be sensitive to the initialization of the embeddings. We have not encountered any problems with the same standard deviation of 0.001 for all datasets. However,

this may not apply in general. While the DCR indicates no privacy issues for the benchmark datasets used, additional caution must be taken when generating synthetic data from privacy sensitive sources. Lastly, our model may be outperformed by other generative models specialized for different types of tabular data, such as time-series.

## **Acknowledgements**

This work used the Dutch national e-infrastructure with the support of the SURF Cooperative using grant no. EINF-7437. We would also like to thank Sander Dieleman for helpful discussions.

## References

- Austin, J., Johnson, D. D., Ho, J., Tarlow, D., and van den Berg, R. Structured Denoising Diffusion Models in Discrete State-Spaces. *arXiv preprint arXiv:2107.03006*, 2021.
- Becker, B. and Kohavi, R. Adult. UCI Machine Learning Repository, 1996. DOI: <https://doi.org/10.24432/C5XW20>.
- Blackard, J. Coverttype. UCI Machine Learning Repository, 1998. DOI: <https://doi.org/10.24432/C50K5N>.
- Borisov, V., Seßler, K., Leemann, T., Pawelczyk, M., and Kasneci, G. Language Models are Realistic Tabular Data Generators. In *International Conference on Learning Representations*, 2023.
- Campbell, A., Benton, J., De Bortoli, V., Rainforth, T., Deligiannidis, G., and Doucet, A. A Continuous Time Framework for Discrete Denoising Models. In *Advances in Neural Information Processing Systems*, volume 35, New Orleans, USA, 2022.
- Chen, S. Beijing PM2.5 Data. UCI Machine Learning Repository, 2017. DOI: <https://doi.org/10.24432/C5JS49>.
- Chen, T. On the Importance of Noise Scheduling for Diffusion Models. *arXiv preprint arXiv:2301.10972*, 2023.
- Chen, T., Zhang, R., and Hinton, G. Analog Bits: Generating Discrete Data using Diffusion Models with Self-Conditioning. *arXiv preprint arXiv:2208.04202*, 2022.
- Clore, J., Cios, K., DeShazo, J., and Strack, B. Diabetes 130-US hospitals for years 1999-2008. UCI Machine Learning Repository, 2014. DOI: <https://doi.org/10.24432/C5230J>.
- Club, L. Loan data from Lending Club, 2015.
- Deb, P. and Trivedi, P. K. Demand for Medical Care by the Elderly: A Finite Mixture Approach. *Journal of Applied Econometrics*, 12(3):313–336, 1997. ISSN 0883-7252, 1099-1255. doi: 10.1002/(SICI)1099-1255(199705)12:3<313::AID-JAE440>3.0.CO;2-G.
- Dhariwal, P. and Nichol, A. Diffusion Models Beat GANs on Image Synthesis. In *Advances in Neural Information Processing Systems*, volume 34, pp. 8780–8794. Curran Associates, Inc., 2021.
- Dieleman, S., Sartran, L., Roshannai, A., Savinov, N., Ganin, Y., Richemond, P. H., Doucet, A., Strudel, R., Dyer, C., Durkan, C., Hawthorne, C., Leblond, R., Grathwohl, W., and Adler, J. Continuous diffusion for categorical data. *arXiv preprint arXiv:2211.15089*, 2022.
- Ding, F., Hardt, M., Miller, J., and Schmidt, L. Retiring Adult: New Datasets for Fair Machine Learning. *arXiv:2108.04884*, 2021.
- Fernandes, K., Vinagre, P., Cortez, P., and Sernadela, P. Online News Popularity. UCI Machine Learning Repository, 2015. DOI: <https://doi.org/10.24432/C5NS3V>.
- Ho, J. and Salimans, T. Classifier-Free Diffusion Guidance. *arXiv preprint arXiv:2207.12598*, 2022.
- Ho, J., Jain, A., and Abbeel, P. Denoising Diffusion Probabilistic Models. In *Advances in Neural Information Processing Systems*, volume 33, pp. 6840–6851. Curran Associates, Inc., 2020.
- Ho, J., Salimans, T., Gritsenko, A., Chan, W., Norouzi, M., and Fleet, D. J. Video Diffusion Models. *arXiv preprint arXiv:2204.03458*, 2022.
- Hoogetboom, E., Nielsen, D., Jaini, P., Forré, P., and Welling, M. Argmax Flows and Multinomial Diffusion: Learning Categorical Distributions. In *Advances in Neural Information Processing Systems*, volume 34, pp. 12454–12465. Curran Associates, Inc., 2021.
- Hoogetboom, E., Satorras, V. G., Vignac, C., and Welling, M. Equivariant Diffusion for Molecule Generation in 3D. In *Proceedings of the 39th International Conference on Machine Learning*, volume 162 of *Proceedings of Machine Learning Research*, pp. 8867–8887, Baltimore, Maryland, USA, 2022. PMLR.

- Hyvärinen, A. Estimation of Non-Normalized Statistical Models by Score Matching. *Journal of Machine Learning Research*, 6(24):695–709, 2005.
- Jabri, A., Fleet, D., and Chen, T. Scalable Adaptive Computation for Iterative Generation. *arXiv preprint arXiv:2212.11972*, 2022.
- Jolicoeur-Martineau, A., Fatras, K., and Kachman, T. Generating and Imputing Tabular Data via Diffusion and Flow-based Gradient-Boosted Trees. In *Proceedings of the 27th International Conference on Artificial Intelligence and Statistics*, volume 238, Valencia, Spain, February 2024. PMLR.
- Karras, T., Aittala, M., Aila, T., and Laine, S. Elucidating the Design Space of Diffusion-Based Generative Models. In *Advances in Neural Information Processing Systems*, volume 35, pp. 26565–26577. Curran Associates, Inc., 2022.
- Karras, T., Aittala, M., Lehtinen, J., Hellsten, J., Aila, T., and Laine, S. Analyzing and Improving the Training Dynamics of Diffusion Models. *arXiv preprint arXiv:2312.02696*, December 2023.
- Keramati, A., Jafari-Marandi, R., Aliannejadi, M., Ahmadian, I., Mozaffari, M., and Abbasi, U. Improved churn prediction in telecommunication industry using data mining techniques. *Applied Soft Computing*, 24:994–1012, 2014. ISSN 1568-4946. doi: <https://doi.org/10.1016/j.asoc.2014.08.041>.
- Kim, J., Lee, C., and Park, N. STaSy: Score-based Tabular data Synthesis. *arXiv preprint arXiv:2210.04018*, 2023.
- Kingma, D. P. and Gao, R. Understanding Diffusion Objectives as the ELBO with Simple Data Augmentation. *arXiv preprint arXiv:2303.00848*, September 2023.
- Kingma, D. P., Salimans, T., Poole, B., and Ho, J. Variational Diffusion Models. *arXiv preprint arXiv:2107.00630*, 2022.
- Kotelnikov, A., Baranchuk, D., Rubachev, I., and Babenko, A. TabDDPM: Modelling Tabular Data with Diffusion Models. In *Proceedings of the 40th International Conference on Machine Learning*, volume 202 of *Proceedings of Machine Learning Research*, pp. 17564–17579. PMLR, 2023.
- Lee, C., Kim, J., and Park, N. CoDi: Co-evolving Contrastive Diffusion Models for Mixed-type Tabular Synthesis. In *Proceedings of the 40th International Conference on Machine Learning*, volume 202, Honolulu, Hawaii, USA, 2023. PMLR.
- Li, X. L., Thickstun, J., Gulrajani, I., Liang, P., and Hashimoto, T. B. Diffusion-LM Improves Controllable Text Generation. *arXiv preprint arXiv:2205.14217*, 2022.
- Lin, J. Divergence Measures Based on the Shannon Entropy. *IEEE Transactions on Information Theory*, 37(1):145–151, 1991.
- Liu, T., Qian, Z., Berrevoets, J., and van der Schaar, M. GOGGLE: Generative Modelling for Tabular Data by Learning Relational Structure. In *International Conference on Learning Representations*, 2023.
- Lu, C., Zhou, Y., Bao, F., Chen, J., Li, C., and Zhu, J. DPM-Solver: A Fast ODE Solver for Diffusion Probabilistic Model Sampling in Around 10 Steps. In *36th Conference on Neural Information Processing Systems*, 2022.
- Meng, C., Choi, K., Song, J., and Ermon, S. Concrete Score Matching: Generalized Score Matching for Discrete Data. In *Advances in Neural Information Processing Systems*, volume 35, pp. 34532–34545. Curran Associates, Inc., 2022.
- Moro, S., Rita, P., and Cortez, P. Bank Marketing. UCI Machine Learning Repository, 2012. DOI: <https://doi.org/10.24432/C5K306>.
- Nichol, A. and Dhariwal, P. Improved Denoising Diffusion Probabilistic Models. In *Proceedings of the 38th International Conference on Machine Learning*, volume 139. PMLR, 2021.

- Patki, N., Wedge, R., and Veeramachaneni, K. The synthetic data vault. In *IEEE International Conference on Data Science and Advanced Analytics (DSAA)*, pp. 399–410, Oct 2016. doi: 10.1109/DSAA.2016.49.
- Prokhorenkova, L., Gusev, G., Vorobev, A., Dorogush, A. V., and Gulin, A. CatBoost: Unbiased boosting with categorical features. In *Advances in Neural Information Processing Systems*, volume 31. Curran Associates, Inc., 2018.
- Qian, Z., Ceber, B.-C., and van der Schaar, M. Synthcity: Facilitating innovative use cases of synthetic data in different data modalities. In *Advances in Neural Information Processing Systems*, volume 36, pp. 3173–3188. Curran Associates, Inc., January 2023.
- Ramdas, A., Garcia, N., and Cuturi, M. On Wasserstein Two Sample Testing and Related Families of Nonparametric Tests. *Entropy*, 19(2), 2017.
- Regol, F. and Coates, M. Diffusing Gaussian Mixtures for Generating Categorical Data. *Proceedings of the AAAI Conference on Artificial Intelligence*, 37(8):9570–9578, 2023. ISSN 2374-3468, 2159-5399. doi: 10.1609/aaai.v37i8.26145.
- Rombach, R., Blattmann, A., Lorenz, D., Esser, P., and Ommer, B. High-Resolution Image Synthesis with Latent Diffusion Models. *arXiv preprint arXiv:2112.10752*, 2022.
- Sohl-Dickstein, J., Weiss, E. A., Maheswaranathan, N., and Ganguli, S. Deep Unsupervised Learning using Nonequilibrium Thermodynamics. In *Proceedings of the 32nd International Conference on Machine Learning*, volume 37, Lille, France, 2015. JMLR.
- Song, Y., Sohl-Dickstein, J., Kingma, D. P., Kumar, A., Ermon, S., and Poole, B. Score-Based Generative Modeling through Stochastic Differential Equations. In *ICLR*, 2021.
- Strudel, R., Tallec, C., Altché, F., Du, Y., Ganin, Y., Mensch, A., Grathwohl, W., Savinov, N., Dieleman, S., Sifre, L., and Leblond, R. Self-conditioned Embedding Diffusion for Text Generation. *arXiv preprint arXiv:2211.04236*, 2022.
- Sun, H., Yu, L., Dai, B., Schuurmans, D., and Dai, H. Score-based Continuous-time Discrete Diffusion Models. *arXiv preprint arXiv:2211.16750*, 2023.
- Vincent, P. A Connection Between Score Matching and Denoising Autoencoders. *Neural Computation*, 23(7):1661–1674, 2011. ISSN 0899-7667, 1530-888X. doi: 10.1162/NECO\_a\_00142.
- Watson, D. S., Blesch, K., Kapar, J., and Wright, M. N. Adversarial random forests for density estimation and generative modeling. In *Proceedings of the 26th International Conference on Artificial Intelligence and Statistics*, volume 206, Valencia, Spain, 2023. PMLR.
- Wu, T., Fan, Z., Liu, X., Gong, Y., Shen, Y., Jiao, J., Zheng, H.-T., Li, J., Wei, Z., Guo, J., Duan, N., and Chen, W. AR-Diffusion: Auto-Regressive Diffusion Model for Text Generation. *arXiv preprint arXiv:2305.09515*, 2023.
- Xu, L., Skoularidou, M., Cuesta-Infante, A., and Veeramachaneni, K. Modeling Tabular Data using Conditional GAN. In *Advances in Neural Information Processing Systems*, volume 12. Curran Associates, Inc., 2019.
- Yeh, I.-C. Default of credit card clients. UCI Machine Learning Repository, 2016. DOI: <https://doi.org/10.24432/C55S3H>.
- Zhao, Z., Kunar, A., Van der Scheer, H., Birke, R., and Chen, L. Y. CTAB-GAN: Effective Table Data Synthesizing. In *Proceedings of the 13th Asian Conference on Machine Learning*, volume 157, pp. 97–112. PMLR, 2021.

## A Loss Calibration

A priori, we let the model be indifferent between features. Therefore, we aim to scale the loss of each feature such that they attain the same loss at the terminal timestep  $t = 1$ . In that case, the signal-to-noise ratio is sufficiently low to approximate a situation in which the model has no information about the data. We are looking for calibrated losses  $\mathcal{L}_{\text{MSE}}^*(x_{\text{cont}}^{(i)}, 1)$  and  $\mathcal{L}_{\text{CE}}^*(x_{\text{cat}}^{(j)}, 1)$  which in expectation achieve a unit loss at  $t = 1$ . This way, the model treats all features equally before having seen any information.

For a single scalar feature and given timestep  $t$ , we can write the empirical denoising score matching loss (see Equation (3)) in the EDM parameterization (Karras et al., 2022) as:

$$\mathcal{L}_{\text{MSE}}(x_{\text{cont}}^{(i)}, t) = \lambda(t) \underbrace{\left( c_{\text{skip}}(t)x_t + c_{\text{out}}(t)F_{\theta}^{(i)} - x_{\text{cont}}^{(i)} \right)^2}_{s_{\theta}(x_t, t)},$$

where  $F_{\theta}^{(i)}$  denotes the neural network output for feature  $i$  that parameterizes the score model  $s_{\theta}$ . The parameters  $c_{\text{skip}}(t) = \sigma_{\text{data}}^2 / (\sigma^2(t) + \sigma_{\text{data}}^2)$  and  $c_{\text{out}}(t) = \sigma(t) \cdot \sigma_{\text{data}} / (\sqrt{\sigma^2(t) + \sigma_{\text{data}}^2})$  depend on  $\sigma(t)$  (and  $\sigma_{\text{data}}$ ) and therefore on timestep  $t$ . For  $t \rightarrow 1$ ,  $\sigma(t)$  approaches the maximum noise level  $\sigma_{\text{cont, max}}$  and  $c_{\text{skip}}(t) \rightarrow 0$  and  $c_{\text{out}}(t) \rightarrow 1$  such that the score model directly predicts the data at high noise levels. For  $t \rightarrow 0$ , the model shifts increasingly towards predicting the error that has been added to the true data. In the EDM parameterization, the explicit timestep weight (used to achieve a unit loss across timesteps at initialization (see Appendix B) is  $\lambda(t) = 1/c_{\text{out}}(t)^2 \approx 1$  for  $t = 1$ .

At the terminal timestep  $t = 1$ , we now have:

$$\begin{aligned} \mathbb{E}_{p(x_{\text{cont}}^{(i)})}[\mathcal{L}_{\text{MSE}}(x_{\text{cont}}^{(i)}, 1)] &= \lambda(1) \mathbb{E}_{p(x_{\text{cont}}^{(i)})} \left( c_{\text{skip}}(1)x_1 + c_{\text{out}}(1)F_{\theta}^{(i)} - x_{\text{cont}}^{(i)} \right)^2, \\ &\approx \mathbb{E}_{p(x_{\text{cont}}^{(i)})} \left( 0 \cdot x_1 + 1 \cdot F_{\theta}^{(i)} - x_{\text{cont}}^{(i)} \right)^2, \\ &= \mathbb{E}_{p(x_{\text{cont}}^{(i)})} \left( F_{\theta}^{(i)} - x_{\text{cont}}^{(i)} \right)^2. \end{aligned}$$

Without information, it is optimal to always predict the average value  $\mathbb{E}_{p(x_{\text{cont}}^{(i)})}[x_{\text{cont}}^{(i)}]$  and thus, the minimum expected loss becomes:

$$\mathbb{E}_{p(x_{\text{cont}}^{(i)})}[\mathcal{L}_{\text{MSE}}(x_{\text{cont}}^{(i)}, 1)] = \mathbb{E}_{p(x_{\text{cont}}^{(i)})} \left( \mathbb{E}_{p(x_{\text{cont}}^{(i)})}[x_{\text{cont}}^{(i)}] - x_{\text{cont}}^{(i)} \right)^2 = \text{Var}[x_{\text{cont}}^{(i)}].$$

Therefore, we have  $\mathcal{L}_{\text{MSE}}^*(x_{\text{cont}}^{(i)}, 1) = \mathcal{L}_{\text{MSE}}(x_{\text{cont}}^{(i)}, 1)$  as long as we standardize  $x_{\text{cont}}^{(i)}$  to unit variance.

For a single categorical feature,  $x_{\text{cat}}^{(j)}$  is distributed according to the proportions  $p_c$  (for categories  $c = 1, \dots, C$ ). The denoising model for score interpolation is trained with the CE loss:

$$\mathcal{L}_{\text{CE}}(x_{\text{cat}}^{(j)}, t) = - \sum_{c=1}^C I(x_{\text{cat}}^{(j)} = c) \log F_{\theta, c}^{(j)},$$

where  $F_{\theta, c}^{(j)}$  denotes the score model's prediction of the class probability at timestep  $t$ . Without information, it is optimal to assign the  $c$ -th category the same proportion as in the training set. At  $t = 1$ , we thus let  $F_{\theta, c}^{(j)} = p_c$  such that the minimum loss equals:

$$\mathbb{E}_{p(x_{\text{cat}}^{(j)})}[\mathcal{L}_{\text{CE}}(x_{\text{cat}}^{(j)}, 1)] = - \mathbb{E}_{p(x_{\text{cat}}^{(j)})} \sum_{c=1}^C I(x_{\text{cat}}^{(j)} = c) \log F_{\theta, c}^{(j)}, \quad (9)$$

$$= - \sum_{c=1}^C \mathbb{E}_{p(x_{\text{cat}}^{(j)})} [I(x_{\text{cat}}^{(j)} = c) \log p_c], \quad (10)$$

$$= - \sum_{c=1}^C p_c \log p_c. \quad (11)$$

We use the training set proportions to compute the normalization constant  $Z_j = -\sum_{c=1}^C p_c \log p_c$  to calibrate the loss for categorical features. Then,

$$\mathbb{E}_{p(x_{\text{cat}}^{(j)})}[\mathcal{L}_{\text{CE}}^*(x_{\text{cat}}^{(j)}, 1)] = \mathbb{E}_{p(x_{\text{cat}}^{(j)})}[\mathcal{L}_{\text{CE}}(x_{\text{cat}}^{(j)}, 1)/Z_j] = 1.$$

We have thus achieved calibrated losses with respect to the terminal timestep  $t = 1$ , that is,  $\mathbb{E}_{p(x_{\text{cont}}^{(i)})}[\mathcal{L}_{\text{MSE}}^*(x_{\text{cont}}^{(i)}, 1)] = \mathbb{E}_{p(x_{\text{cat}}^{(j)})}[\mathcal{L}_{\text{CE}}^*(x_{\text{cat}}^{(j)}, 1)] = 1$  for all continuous features  $i$  and categorical features  $j$ .

## B Output Layer Initialization

At initialization, we want the neural network to reflect the state of no information (see Appendix A). Likewise, our goal is a loss of one across all features and timesteps.

For continuous features  $i$ , we initialize the output layer weights (and biases) to zero such that the output of the score model for a single continuous feature,  $F_{\theta}^{(i)}$ , is also zero. Since we use the EDM parameterization (Karras et al., 2022), we apply the associated explicit timestep weight  $\lambda(t) = \frac{\sigma^2(t) + \sigma_{\text{data}}^2}{(\sigma(t) \cdot \sigma_{\text{data}})^2}$ . This is explicitly designed to achieve a unit loss across timesteps at initialization and we show this analytically below. We denote the variances of the data  $x_{\text{cont}}^{(i)}$  and of the Gaussian noise  $\epsilon$  at time  $t$  as  $\sigma_{\text{data}}^2$  and  $\sigma^2(t)$ , respectively.

$$\begin{aligned} \mathbb{E}_{p(x_{\text{cont}}^{(i)}), p(\epsilon)}[\mathcal{L}_{\text{MSE}}^*(x_{\text{cont}}^{(i)}, t)] &= \lambda(t) \mathbb{E}_{p(x_{\text{cont}}^{(i)}), p(\epsilon)} \left( c_{\text{skip}}(t)(x_{\text{cont}}^{(i)} + \epsilon) + c_{\text{out}}(t)F_{\theta}^{(i)} - x_{\text{cont}}^{(i)} \right)^2, \\ &= \lambda(t) \mathbb{E}_{p(x_{\text{cont}}^{(i)}), p(\epsilon)} \left( c_{\text{skip}}(t)(x_{\text{cont}}^{(i)} + \epsilon) - x_{\text{cont}}^{(i)} \right)^2, \\ &= \frac{\sigma^2(t) + \sigma_{\text{data}}^2}{(\sigma(t) \cdot \sigma_{\text{data}})^2} \mathbb{E}_{p(x_{\text{cont}}^{(i)}), p(\epsilon)} \left( \frac{\sigma_{\text{data}}^2}{\sigma^2(t) + \sigma_{\text{data}}^2} (x_{\text{cont}}^{(i)} + \epsilon) - x_{\text{cont}}^{(i)} \right)^2, \\ &= \frac{\sigma^2(t) + \sigma_{\text{data}}^2}{(\sigma(t) \cdot \sigma_{\text{data}})^2} \mathbb{E}_{p(x_{\text{cont}}^{(i)}), p(\epsilon)} \left( \frac{\sigma_{\text{data}}^2 \epsilon - \sigma^2(t)x_{\text{cont}}^{(i)}}{\sigma^2(t) + \sigma_{\text{data}}^2} \right)^2, \\ &= \frac{1}{\sigma^2(t) + \sigma_{\text{data}}^2} \mathbb{E}_{p(x_{\text{cont}}^{(i)}), p(\epsilon)} \left( \frac{\sigma_{\text{data}}}{\sigma(t)} \epsilon - \frac{\sigma(t)}{\sigma_{\text{data}}} x_{\text{cont}}^{(i)} \right)^2, \\ &= \frac{1}{\sigma^2(t) + \sigma_{\text{data}}^2} \mathbb{E}_{p(x_{\text{cont}}^{(i)}), p(\epsilon)} \left( \frac{\sigma_{\text{data}}^2}{\sigma^2(t)} \epsilon^2 + \frac{\sigma^2(t)}{\sigma_{\text{data}}^2} (x_{\text{cont}}^{(i)})^2 - 2\epsilon x_{\text{cont}}^{(i)} \right), \\ &= \frac{1}{\sigma^2(t) + \sigma_{\text{data}}^2} \left( \frac{\sigma_{\text{data}}^2}{\sigma^2(t)} \underbrace{\text{Var}(\epsilon)}_{\sigma^2(t)} + \frac{\sigma^2(t)}{\sigma_{\text{data}}^2} \underbrace{\text{Var}(x_{\text{cont}}^{(i)})}_{\sigma_{\text{data}}^2} - 2 \underbrace{\text{Cov}(\epsilon, x_{\text{cont}}^{(i)})}_0 \right), \\ &= \frac{1}{\sigma^2(t) + \sigma_{\text{data}}^2} (\sigma_{\text{data}}^2 + \sigma^2(t)) = 1. \end{aligned}$$

For categorical features  $j$ , we initialize the output layer such that the model achieves the respective losses under no information. Using the loss normalization constant  $Z_j$  (see Appendix A) and dropping the expectation over  $p(\epsilon)$ , we have

$$\mathbb{E}_{p(x_{\text{cat}}^{(j)})}[\mathcal{L}_{\text{CE}}^*(x_{\text{cat}}^{(j)}, t)] = \mathbb{E}_{p(x_{\text{cat}}^{(j)})}[\mathcal{L}_{\text{CE}}(x_{\text{cat}}^{(j)}, t)/Z_j] = \frac{1}{Z_j} \mathbb{E}_{p(x_{\text{cat}}^{(j)})}[\mathcal{L}_{\text{CE}}(x_{\text{cat}}^{(j)}, t)].$$

Hence, for  $\mathbb{E}_{p(x_{\text{cat}}^{(j)})}[\mathcal{L}_{\text{CE}}(x_{\text{cat}}^{(j)}, t)] = Z_j$ , we obtain an expected loss of one irrespective of  $t$ . The neural network outputs a vector of logits  $F_{\theta}^{(j)}$  that are transformed into probabilities with a softmax function for each categorical feature. We denote the  $c$ -th element of that vector  $\text{softmax}(\cdot)_c$ . Since  $Z_j$  is derived in Equation (11) by imposing probabilities equal to the training set proportions for that category,  $p_c$ , we have

$$\log p_c = \log \text{softmax}(F_{\theta}^{(j)})_c = \log \frac{\exp(F_{\theta, c}^{(j)})}{\sum_{k=1}^C \exp(F_{\theta, k}^{(j)})} = F_{\theta, c}^{(j)} - \log \sum_{k=1}^C \exp(F_{\theta, k}^{(j)}).$$

We initialize the neural network such that  $F_{\theta,c}^{(j)} = \log p_c$  for all  $c$ . This can be achieved by initializing the output layer weights to zero and the output layer biases to the relevant training set log-proportions of the corresponding class. Hence, this initialization gives us

$$F_{\theta,c}^{(j)} - \log \sum_{k=1}^C \exp(F_{\theta,k}^{(j)}) = \log p_c - \log \sum_{k=1}^C p_k = \log p_c,$$

which in turn leads to an initial loss of  $Z_j$  for all  $t$  and therefore achieves a uniform, calibrated loss of one at initialization similar to the continuous feature case.

## C Adaptive Normalization of the Average Diffusion Loss

Both the loss calibration (see Appendix A) and output layer initialization (see Appendix B) ensure that the losses across timesteps (and features) are equal *at* initialization. During training, the adaptive noise schedules allow the model to focus automatically on the noise levels that matter most, i.e., where the loss increase is steepest. However, the better the model becomes at a given timestep  $t$ , the lower the loss at that timestep, and the lower the gradient signal relative to the signal received for timesteps  $\tilde{t} > t$ . To counteract this, we additionally use an adaptive normalization of the average diffusion loss (averaged over the features) across timesteps. Specifically, we want to weight the average diffusion loss at timestep  $t$ ,  $\mathcal{L}(t)$  given in Equation (6), such that the normalized loss is the same (equal to one) for all  $t$ . Similar methods have been used by Karras et al. (2023) and Kingma & Gao (2023), we follow the latter in the setup of the corresponding network.

We train a neural network alongside our diffusion model to predict  $\mathcal{L}(t)$  based on  $t$  and using the MSE loss to learn this weighting. In particular, we first compute  $c_{\text{noise}}(t) = \log(t)/4$  following the EDM parameterization (Karras et al., 2022). Then, we embed  $c_{\text{noise}}$  in frequency space (1024-dimensional) using Fourier features. The result is then passed through a single linear layer to output a scalar value, which is in turn passed through an exponential function to ensure that the prediction  $\hat{\mathcal{L}}(t) \geq 0$ . We initialize the weights and biases to zero, to ensure that at model initialization we have a unit normalization.

## D Derivation of the Functional Timewarping Form

Since higher noise levels,  $\sigma$ , imply a lower signal-to-noise ratio and, in turn, a larger loss,  $\ell$ , we know that the loss must be a monotonically increasing and S-shaped function of the noise level. Additionally, the function has to be easy to invert and differentiate. We incorporate this prior information in the functional timewarping form of  $F : \sigma \mapsto \ell$ . A convenient choice is the cdf of the logistic distribution:

$$F_{\log}(y) = [1 + \exp(-\nu(y - \mu^*))]^{-1}, \quad (12)$$

where  $\mu^*$  describes the location of the inflection point of the S-shaped function and  $\nu \geq 1$  indicates the steepness of the curve.

We let  $y = \text{logit}(\sigma) = \log(\sigma/(1 - \sigma))$  to change the domain of  $F_{\log}$  from  $(-\infty, \infty)$  to  $(0, 1)$ . The latter covers all possible values of the noise level  $\sigma$  scaled to  $[0, 1]$  with the pre-specified minimum and maximum noise levels  $\sigma_{\min}$  and  $\sigma_{\max}$ . To define the parameter  $\mu$  in the same space and ensure that  $0 < \mu < 1$ , we also let  $\mu^* = \text{logit}(\mu)$ . Accordingly, we derive the cdf of the *domain-adapted* Logistic distribution:

$$F_{\text{d.a.log}}(\sigma) = \left[ 1 + \left( \frac{\sigma}{1 - \sigma} \frac{1 - \mu}{\mu} \right)^{-\nu} \right]^{-1}. \quad (13)$$

Since  $\ell$  is not bounded, we introduce a multiplicative scale parameter,  $\gamma > 0$ , such that for timewarping we predict the potentially feature-specific loss as  $\hat{\ell} = F(\sigma) = \gamma F_{\text{d.a.log}}(\sigma)$ .  $F_{\text{d.a.log}}$  can also be initialized to the cdf of the uniform distribution with  $\mu = 0.5$ ,  $\nu \approx 1$  and  $\gamma = 1$  such that all noise levels are initially equally weighted. However, an initial overweighting of lower noise levels is beneficial for tabular data (see also Section 3.4).



Likewise, we can derive the inverse cdf  $F_{\text{d.a.log}}^{-1}(t)$ , that is our mapping of interest from timestep  $t$  to noise level  $\sigma$ , in closed form:

$$\sigma = F_{\text{d.a.log}}^{-1}(t) = \text{sigmoid}(c), \text{ with } c = \ln\left(\frac{\mu}{1-\mu}\right) + \frac{1}{\nu} \ln\left(\frac{t}{1-t}\right). \quad (14)$$

When training the diffusion model, we learn the parameters of  $F_{\text{d.a.log}}$  as well as  $\gamma$  by predicting the diffusion loss using  $F(\sigma)$  and the noise levels scaled to  $[0, 1]$ . At the beginning of each training step, we then use the current state of the parameters and  $F_{\text{d.a.log}}^{-1}$ , with a sampled timestep  $t \sim \mathcal{U}_{[0,1]}$  as input, to derive  $\sigma$ . To allow for *feature-specific*, adaptive noise schedules, we separately introduce  $F_k(\sigma_k)$  for each feature  $k$ , to predict the feature-specific loss  $\ell_k$  based on the feature-specific scaled noise level  $\sigma_k$ .

Note that with timewarping we create a feedback loop in which we generate more and more  $\sigma$ s from the region of interest, decreasing the number of observations available to learn the parameters in different noise level regions. We thus weight the timewarping loss,  $\|\ell - \hat{\ell}\|_2^2$ , when fitting  $F(\sigma)$  to the data by the reciprocal of the pdf  $f_{\text{d.a.log}}(\sigma)$  to mitigate this adverse effect (see Dieleman et al., 2022). Again, this function is available to us in closed form. With  $F_{\text{log}}$  and  $f_{\text{log}}$  denoting the respective cdf and pdf of the Logistic distribution, we have

$$\begin{aligned} f_{\text{d.a.log}}(\sigma) &= \frac{\partial}{\partial y} F_{\text{log}}(y) \Big|_{y=\text{logit}(\sigma)} \frac{\partial}{\partial \sigma} \ln \frac{\sigma}{1-\sigma} \\ &= f_{\text{log}}(\text{logit}(\sigma)) \frac{1}{\sigma(1-\sigma)} \\ &= \frac{\nu}{\sigma(1-\sigma)} \cdot \frac{Z(\sigma, \mu, \nu)}{(1 + Z(\sigma, \mu, \nu))^2}, \end{aligned}$$

where we defined  $Z(\sigma, \mu, \nu) = \left(\frac{\sigma}{1-\sigma} \frac{1-\mu}{\mu}\right)^{-\nu}$  and used the definitions of  $f_{\text{log}}$  and the parameter  $\mu^*$ .

## E Datasets

Our selected benchmark datasets are highly diverse, particularly in the number of categories for a categorical feature. Almost all datasets are licensed under creative commons that permits their usage in our research. Only the `nmes` dataset license is unknown but the data is publicly accessible on the author’s website.

For the `diabetes` and `covertime` datasets, we transform the original multi-class classification problem into a binary classification task for easier comparison. For the `covertime` data, the task is converted into predicting whether a forest of type 2 is present in a given  $30 \times 30$  meter area. In the `diabetes` data, we convert the task by predicting whether a patient was readmitted to a hospital.

Table 3: Overview of the selected experimental datasets. We count the outcome towards the respective features that remain after removing continuous features with an excessive number of missings. The minimum and maximum number of categories are taken over all categorical features.

Dataset	License	Prediction task	Total no. observations	No. of features		No. of categories	
				categorical	continuous	min.	max.
<code>acsincome</code> (Ding et al., 2021)	CC0	regression	1 664 500	8	3	2	529
<code>adult</code> (Becker & Kohavi, 1996)	CC BY 4.0	binary classification	48 842	9	6	2	42
<code>bank</code> (Moro et al., 2012)	CC BY 4.0	binary classification	41 188	11	10	2	12
<code>beijing</code> (Chen, 2017)	CC BY 4.0	regression	41 757	1	10	4	4
<code>churn</code> (Keramati et al., 2014)	CC BY 4.0	binary classification.	3 150	5	9	2	5
<code>covertime</code> (Blackard, 1998)	CC BY 4.0	binary classification	581 012	44	10	2	2
<code>default</code> (Yeh, 2016)	CC BY 4.0	binary classification	30 000	10	14	2	11
<code>diabetes</code> (Clare et al., 2014)	CC BY 4.0	binary classification	101 766	28	9	2	716
<code>lending</code> (Club, 2015)	DbCL 1.0	regression	9 182	10	34	2	3151
<code>news</code> (Fernandes et al., 2015)	CC BY 4.0	regression	39 644	14	46	2	2
<code>nmes</code> (Deb & Trivedi, 1997)	unknown	regression	4 406	8	11	2	4

## F Baseline Models

Below, we give a brief description of the used generative baseline models (including code sources).

**ARF** (Watson et al., 2023) – a recent generative approach that is based on a random forest for density estimation. The implementation is available at <https://github.com/bips-hb/arfpy> and licensed under the MIT license. We use package version 0.1.1. For training, we utilize 16 CPU cores.

**CTGAN** (Xu et al., 2019) – one of the most popular Generative-Adversarial-Network-based models for tabular data. The implementation is available as part of the Synthetic Data Vault (Patki et al., 2016) at <https://github.com/sdv-dev/CTGAN> and licensed under the Business Source License 1.1. We use package version 0.9.0.

**TVAE** (Xu et al., 2019) – a Variational-Autoencoder-based model for tabular data. Similar to CTGAN. The implementation is available as part of the Synthetic Data Vault (Patki et al., 2016) at <https://github.com/sdv-dev/CTGAN> and licensed under the Business Source License 1.1. We use package version 0.9.0. Note that since we only use TVAE (and CTGAN) as benchmark, and do not provide a synthetic data creation service, the license permits the free usage.

**TabDDPM** (Kotelnikov et al., 2023) – a diffusion-based generative model for tabular data that combines multinomial diffusion (Hoogeboom et al., 2021) and diffusion in continuous space. An implementation is available as part of the `synthcity` package (Qian et al., 2023) at <https://github.com/vanderschaarlab/synthcity/> and licensed under the Apache 2.0 license. We use package version 0.2.7 with slightly adjusted code to allow for the manual specification of categorical features.

**CoDi** (Lee et al., 2023) – a diffusion model trained using an additional contrastive loss, and which factorizes the joint distribution of mixed-type tabular data into a distribution for continuous data conditional on categorical features and a distribution for categorical data conditional on continuous features. Similar to TabDDPM, the authors utilize the multinomial diffusion framework (Hoogeboom et al., 2021) to model categorical data. An implementation is available at <https://github.com/ChaejeongLee/CoDi> under an unknown license.

## G Implementation Details

Each of the selected benchmark models requires a rather different, more specialized neural network architecture. Imposing the same architecture across models is therefore not possible. The same inability holds for the comparison of CDTD to other diffusion-based models: Our model is the first to use a continuous noise distribution on both continuous and categorical features, and therefore the alignment of important design choices, like the noise schedule, across models is not possible. In particular, the Markov transition matrices based forward process of the multinomial diffusion framework (Hoogeboom et al., 2021) in TabDDPM and CoDi does not translate to our setting.

To ensure a fair comparison in terms of sampling steps, we set the steps for CDTD, TabDDPM and CoDi to  $\max(200, \text{default})$ . We therefore increase the default number of sampling steps for CoDi (from 50 steps) and TabDDPM (from 100 steps for classification datasets). For TabDDPM and regression datasets, we use the suggested default of 1000 sampling steps.

We adjust each architecture to a total of  $\pm 3$  million trainable parameters on the `adult` dataset to improve the comparability further (see Table 4) and use the same architectures for all considered datasets. Note that the total number of parameters may vary slightly across datasets due to different number of features and categories affecting the onehot encoding but is still comparable across models. We also align the embedding/bottleneck dimensions for CTGAN, TVAE, TabDDPM and CDTD to 256 to accommodate more complex datasets. If applicable, all models are trained for 30k steps on a single RTX 4090 instance, using PyTorch version 2.2.2.

Table 4: Total number of trainable parameters per model on the `adult` dataset.

Model	Trainable parameters
CTGAN	3 000 397
TVAE	2 996 408
TabDDPM	3 003 924
CoDi	2 998 043
CDTD (per type schedule, TabDDPM architecture)	2 999 721

Below, we briefly discuss our model-specific hyperparameter choices.

**ARF** (Watson et al., 2023): We use the authors’s suggested default hyperparameters. In particular, we use 20 trees,  $\delta = 0$  and a minimum node size of 5. We follow the official package implementation and set the maximum number of iterations to 10 (see <https://github.com/bips-hb/arfp>).

**CTGAN** (Xu et al., 2019): We follow the popular implementation in the Synthetic Data Vault package (see <https://github.com/sdv-dev/CTGAN>). For this model to work, the batch size must be divisible by 10. Therefore, we adjust the batch size if necessary. We use a 258-dimensional embedding (instead of the default embedding dimension of 128) to better align the CTGAN architecture with TVAE, TabDDPM and CDCD.

**TVAE** (Xu et al., 2019): We again follow the implementation in the Synthetic Data Vault. We use a 258-dimensional embedding to better align the architecture with CTGAN, TabDDPM and CDCD.

**TabDDPM** (Kotelnikov et al., 2023): There are no general default hyperparameters provided. Hence, we mostly adapt the papers’ tuned hyperparameters for the `adult` dataset (one of the few used datasets that includes both continuous and categorical features). However, we decrease the learning rate from 0.002 to 0.001, since most of the tuned models in the paper used learning rates around 0.001. For regression task datasets, we use 1000 sampling steps in accordance with the author’s settings. For classification task datasets, we use 200 sampling steps (instead of the default 100 steps), to better align the model with CoDi and CDCD. Note also that for classification task datasets, TabDDPM models the conditional distribution  $p(x|y)$ , instead of the unconditional distribution  $p(x)$  which is modeled for regression tasks. We adjust the dimension of the bottleneck to 256 (instead of the default 128) to also accommodate also larger datasets and align the model with CTGAN, TVAE, and CDCD.

**CoDi** (Lee et al., 2023): We use the default hyperparameters from the official code (see <https://github.com/ChaejeongLee/CoDi>).

**CDTD** (ours): To ensure comparability in particular to TabDDPM and CoDi, we use the same neural network architecture as TabDDPM. We only change the input layers to accommodate our embedding-based framework. In the input layer, we vectorize all embedded categorical features and concatenate them with the scalar valued continuous features. The adjusted output layer ensures that we predict a single value for each continuous features and set of class-specific probabilities for each categorical feature. Since our use of embeddings introduces additional parameters, we scale the hidden layers slightly down relative to the TabDDPM to ensure approximately 3 million trainable parameters (instead of 808 neurons per layer we use 806) on the `adult` dataset. More details on the CDTD implementation are given in Appendix J.

## H Tuning of the Detection Model

We use a catboost model (Prokhorenkova et al., 2018) to test whether real and generated samples can be distinguished. We generate the same number of fake observations for each of the real train, validation and test sets. We cap the maximum size of the real data subsets to 25 000, and subsample them if necessary, to limit the computational load. We then combine real and fake observations per set to  $\mathcal{D}_{\text{train}}^{\text{detect}}$ ,  $\mathcal{D}_{\text{valid}}^{\text{detect}}$ , and  $\mathcal{D}_{\text{test}}^{\text{detect}}$ , respectively. The catboost model is trained on  $\mathcal{D}_{\text{train}}^{\text{detect}}$  with the task of predicting whether an observation is real or fake. We tune the catboost model with optuna and for 50 trials to maximize the accuracy on  $\mathcal{D}_{\text{valid}}^{\text{detect}}$ . The catboost hyperparameter search space is given in Table 5. Afterwards, we repeat the sampling process and the creation of  $\mathcal{D}_{\text{train}}^{\text{detect}}$ ,  $\mathcal{D}_{\text{valid}}^{\text{detect}}$  and  $\mathcal{D}_{\text{test}}^{\text{detect}}$  for five different seeds. Each time, the model is trained on  $\mathcal{D}_{\text{train}}^{\text{detect}}$  with the previously tuned hyperparameters, and evaluated on  $\mathcal{D}_{\text{test}}^{\text{detect}}$ . The average test set accuracy over the five seeds yields the estimated detection score.

Table 5: Catboost hyperparameter space settings. The model is tuned for 50 trials.

Parameter	Distribution
no. iterations	= 1000
learning rate	Log Uniform [0.001, 1.0]
depth	Cat([3,4,5,6,7,8])
L2 regularization	Uniform [0.1, 10]
bagging temperature	Uniform [0, 1]
leaf estimation iters	Integer Uniform [1, 10]

## I Machine Learning Efficiency Models

For the group of machine learning efficiency models, we use the scikit-learn and catboost package implementations including the default parameter settings, if not specified otherwise below:

**Logistic or Ridge Regression:** max. iterations = 1000

**Random Forest:** max. depth = 12, no. estimators = 100

**Catboost:** no. iterations = 2000, early stopping rounds = 50, overfitting detector pval = 0.001

## J CDTD Implementation Details

To enable a fair comparison to the other methods and in particular TabDDPM, the CDTD score model utilizes the exact same architecture and optimizer as Kotelnikov et al. (2023). An overview of the score model is given in Figure 4: First, the noisy data, including the noisy scalars for continuous features and the noisy embeddings for categorical features, are projected onto a 256-dimensional space. Similarly, timestep  $t$  and possibly conditioning information  $y$  are embedded in the same space. All 256-dimensional vectors are then added and the results is processed by a set of five fully-connected linear layers with ReLU activation functions. Lastly, a linear projection maps the output of the fully-connected layers to the required output dimensions, which depend on the number of features and number of categories per feature.

The only major difference to the TabDDPM setup are the inputs, as we need to embed the categorical features in Euclidean space. The output dimensions are the same, as we need to predict a single scalar for each  $x_{\text{cont},i}$ , and  $|C_j|$  values for each  $x_{\text{cat},j}$ , with  $C_j$  the set of categories of feature  $j$ . We change the initialization of the output layer as described in Appendix B: To handle our inputs, we embed the categorical features in 16-dimensional space and add a feature-specific bias of the same dimension, which captures feature-specific information common to all categories and is initialized to zero. We  $L_2$ -normalize each embedding to prevent a degenerate embedding space in which embeddings are pushed further and further apart (see Dieleman et al., 2022). Also, Dieleman et al. (2022) argue that the standard deviation of the Normal distribution used to initialize the embeddings, denoted by  $\sigma_{\text{cat emb}}$ , is an important hyperparameter. In this paper, we set  $\sigma_{\text{cat emb}} = 0.001$  for all datasets and have not seen detrimental effects. Tuning this hyperparameter in practice could improve the results further.

Since we utilize embeddings, we have to scale the neurons per layer slightly down in the stack of the five fully-connected layers (from 808 for TabDDPM to 806). Also, since TabDDPM samples discrete steps from  $[0, T]$ , with  $T \gg 1$ , we adjust our timesteps  $t \in [0, 1]$  up by 1000. We use the same optimizer (Adam), learning rate (0.001), learning rate decay (linear), EMA decay (0.999), and

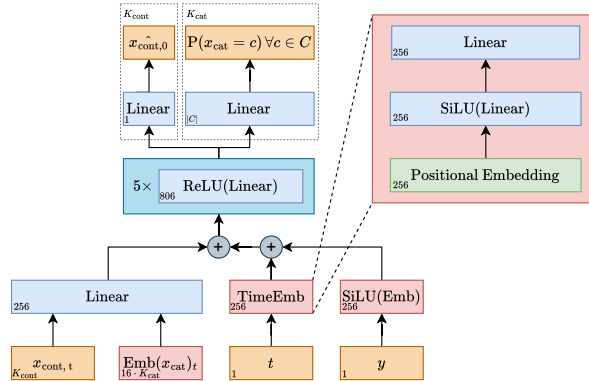


Figure 4: Overview of the CDTD architecture adapted from TabDDPM. The dimensions of the inputs and layer outputs are stated in the lower-left hand corner for a continuous features  $x_{\text{cont}}$  and a categorical features  $x_{\text{cat}}$ . Note that each categorical features can have a different number of categories  $|C|$ , impacting the output dimension of the final layer. Scalars are colored orange, embeddings red and linear layers blue. The positional embedding highlighted in green refers to the positional sinusoidal embedding. CDTD only conditions on  $y$ , i.e., the target feature, for classification task datasets.

training steps (30000). However, since we work with embeddings we add a linear warmup schedule over the first 100 steps.

Instead of using the vanilla uniform (time)step sampling as the TabDDPM, the CDTD model uses antithetic sampling Dieleman et al. (2022); Kingma et al. (2022). The timesteps are still uniformly distributed but spread out more evenly over the domain, which benefits the training of the adaptive noise schedules. For generation, we use an Euler sampler with 200 steps to minimize the discretization error.

## K Examples of Learned Noise Schedules

Below we show the learned noise schedules for the smallest dataset (churn) and the largest dataset (accincome). We also illustrate how well single, per type and per feature schedules fit the respective losses for each of the datasets.

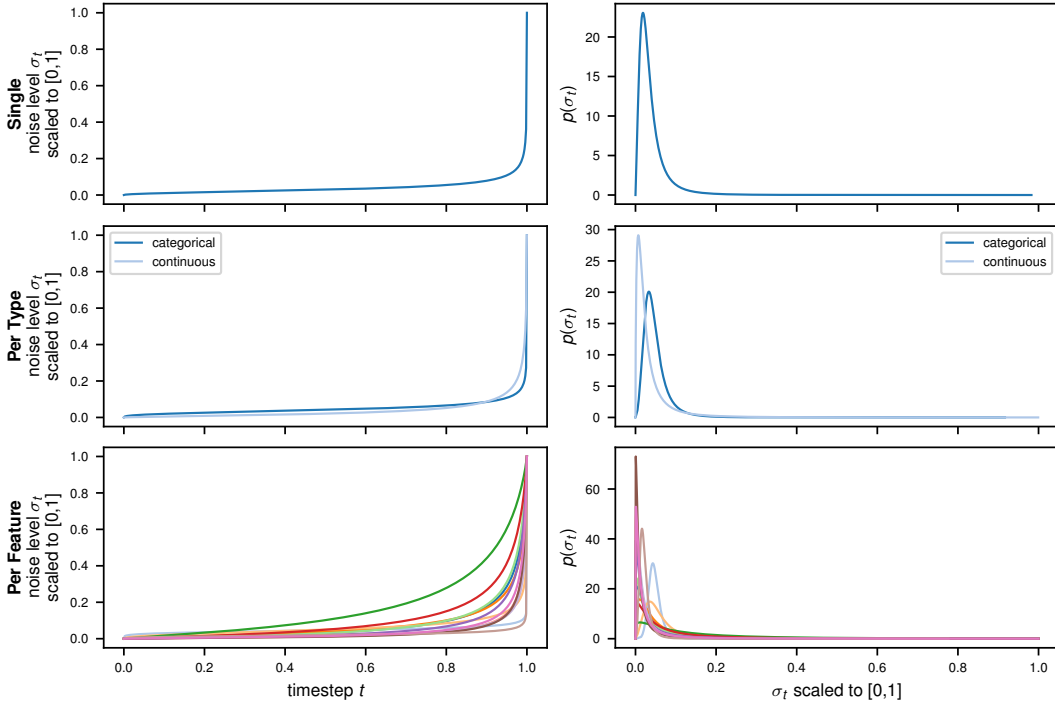


Figure 5: (Left): Learned noise schedules for churn. This reflects  $F_{d.a.log,k}^{-1}$ . (Right): Implicit weighting of noise levels / timesteps. This visualizes  $f_{d.a.log,k}$ .

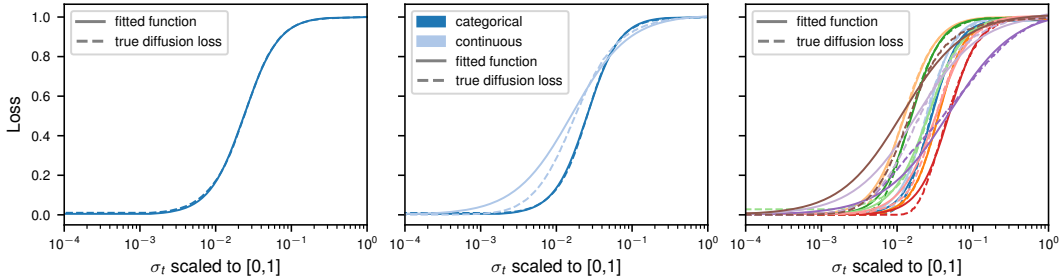


Figure 6: Illustration of the goodness of fit of the timewarping function  $F_k$  for single (left), per type (middle) and per feature noise schedules (right) on the accincome data.

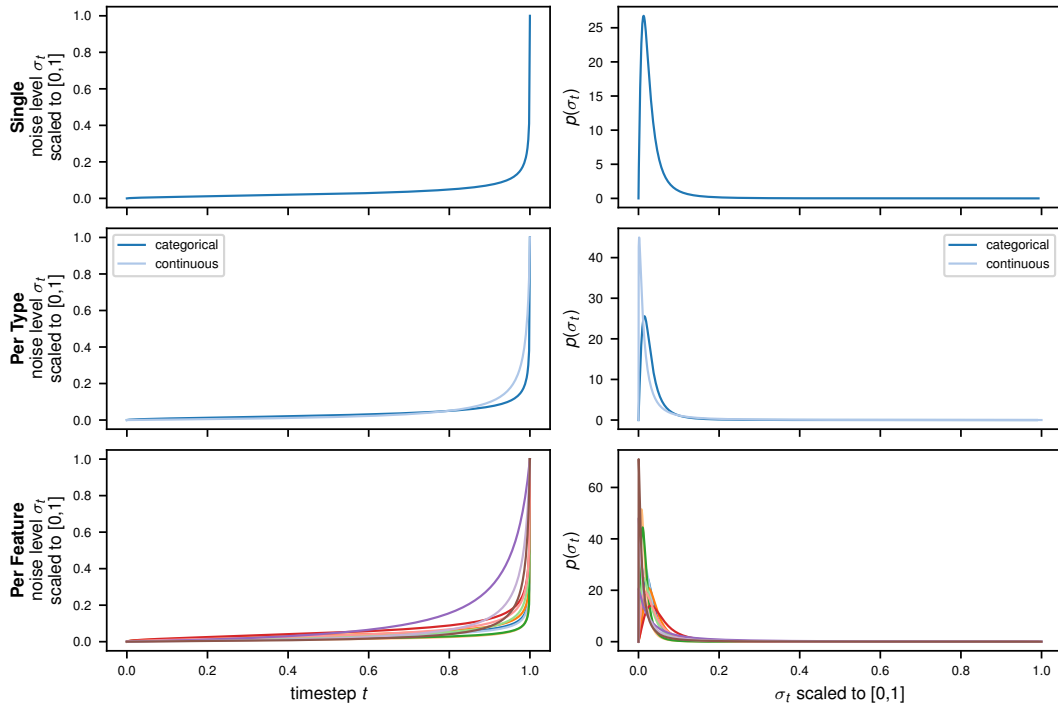


Figure 7: (Left): Learned noise schedules for `accincome`. This reflects  $F_{\text{d.a.log},k}^{-1}$ . (Right): Implicit weighting of noise levels / timesteps. This visualizes  $f_{\text{d.a.log},k}$ .

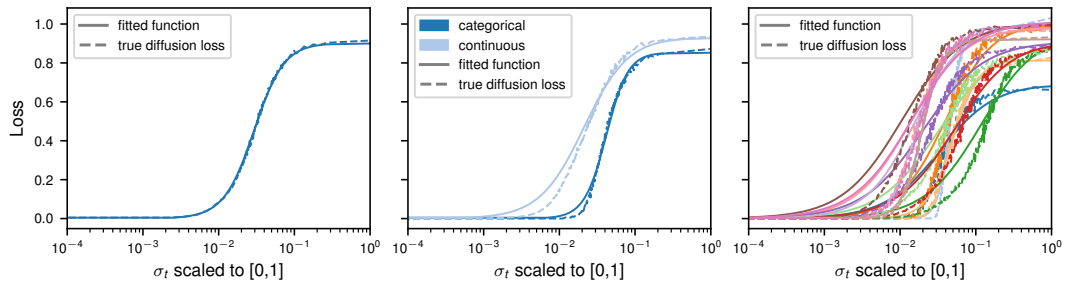


Figure 8: Illustration of the goodness of fit of the timewarping function  $F_k$  for single (left), per type (middle) and per feature noise schedules (right) on the churn data.

## L Qualitative Comparisons

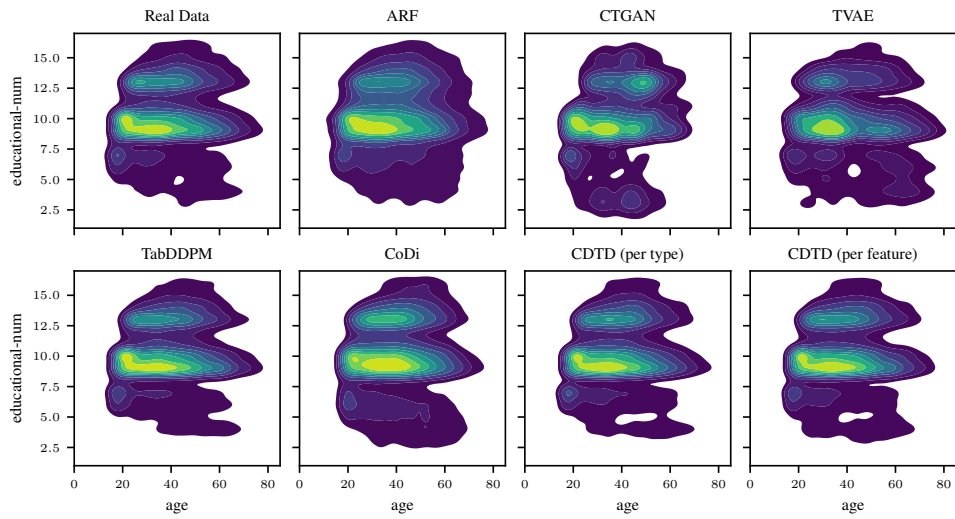


Figure 9: Bivariate density for age and educational-num from the adult data.

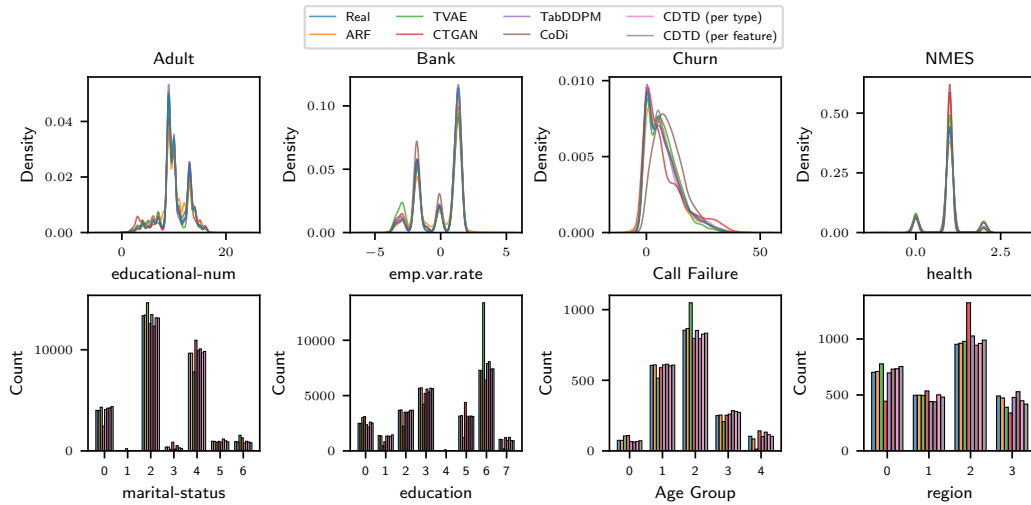


Figure 10: Qualitative comparison of some univariate distributions for adult, bank, churn, nmes data.

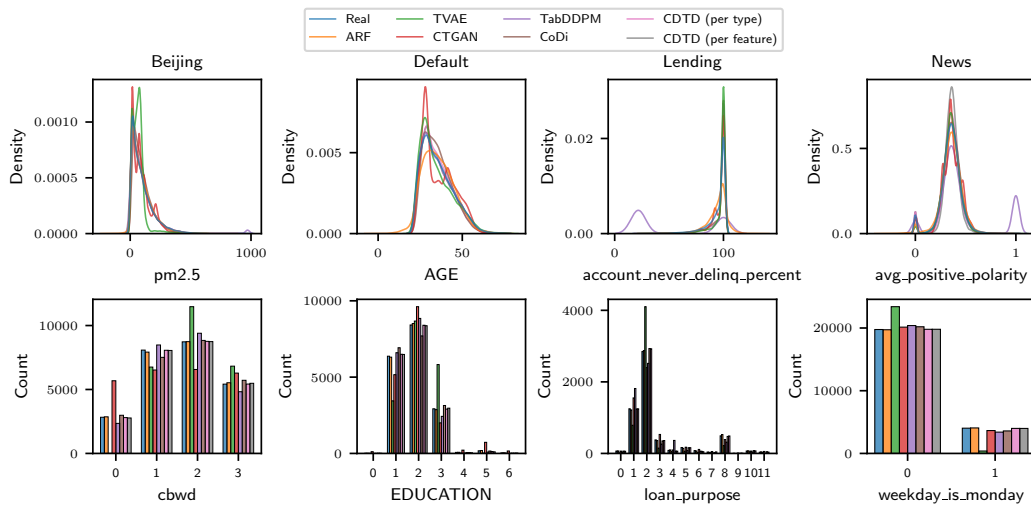


Figure 11: Qualitative comparison of some univariate distributions for beijing, default, lending, news data. Note that CoDi is excluded from lending as it is prohibitively expensive to train on this dataset.



## M Visualizations of Captured Correlations

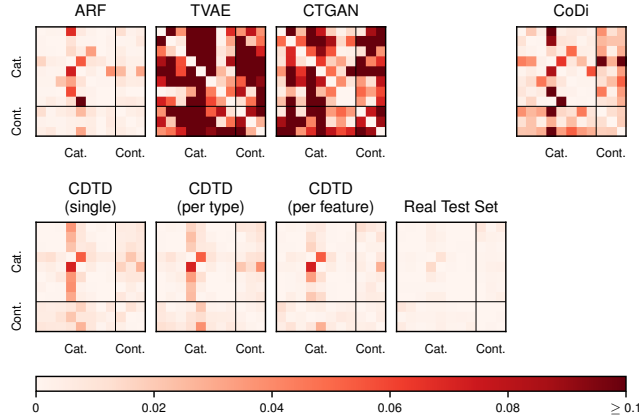


Figure 12: Element-wise absolute differences of the correlation matrices between the real training set and the synthetic data for the `acsincome` dataset. TabDDPM generates NaNs for this dataset and is therefore excluded. Continuous (cont.) and categorical (cat.) features are indicated on the axes.

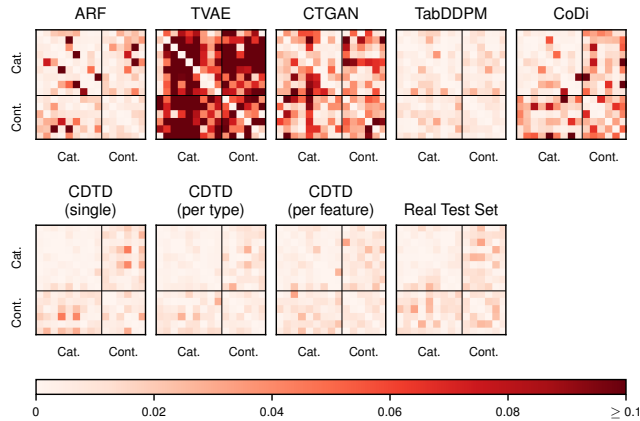


Figure 13: Element-wise absolute differences of the correlation matrices between the real training set and the synthetic data for the `adult` dataset. Continuous (cont.) and categorical (cat.) features are indicated on the axes.

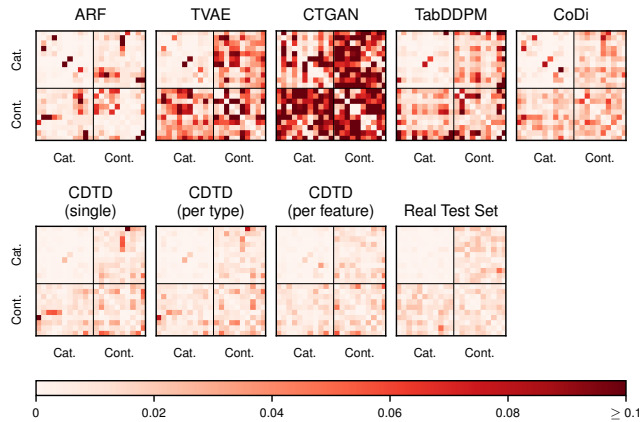


Figure 14: Element-wise absolute differences of the correlation matrices between the real training set and the synthetic data for the `bank` dataset. Continuous (cont.) and categorical (cat.) features are indicated on the axes.

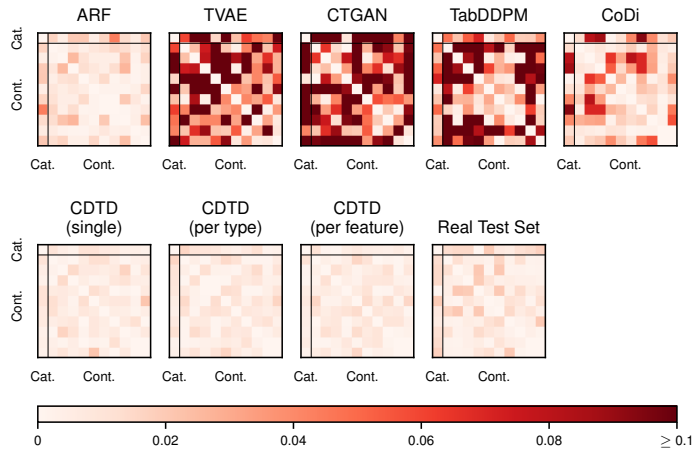


Figure 15: Element-wise absolute differences of the correlation matrices between the real training set and the synthetic data for the beijing dataset. Continuous (cont.) and categorical (cat.) features are indicated on the axes.

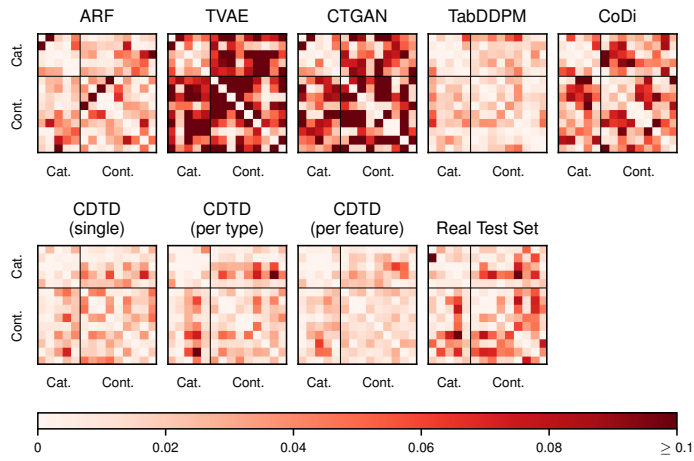


Figure 16: Element-wise absolute differences of the correlation matrices between the real training set and the synthetic data for the churn dataset. Continuous (cont.) and categorical (cat.) features are indicated on the axes.

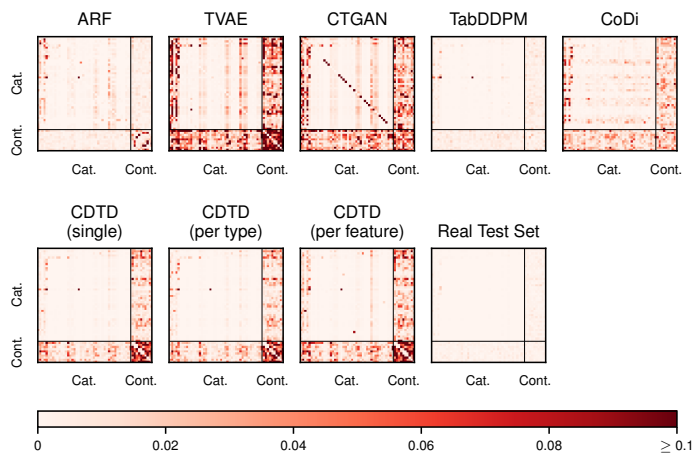


Figure 17: Element-wise absolute differences of the correlation matrices between the real training set and the synthetic data for the covertype dataset. Continuous (cont.) and categorical (cat.) features are indicated on the axes.

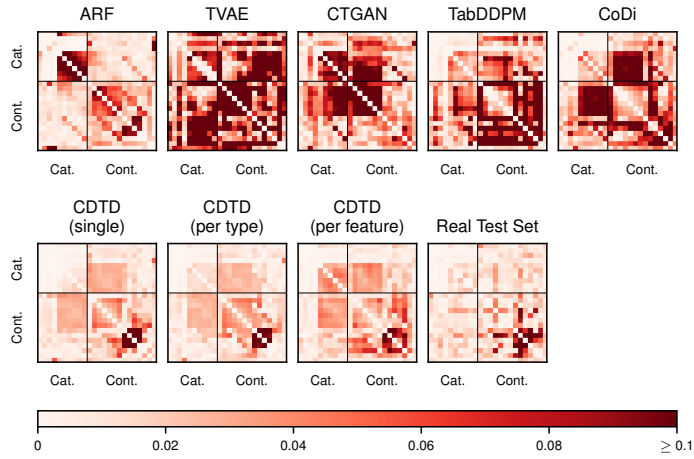


Figure 18: Element-wise absolute differences of the correlation matrices between the real training set and the synthetic data for the default dataset. Continuous (cont.) and categorical (cat.) features are indicated on the axes.

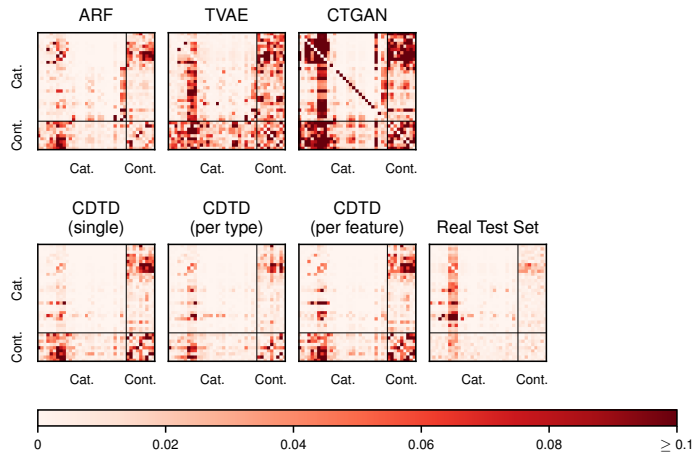


Figure 19: Element-wise absolute differences of the correlation matrices between the real training set and the synthetic data for the diabetes dataset. TabDDPM generates NaNs for this dataset and is therefore excluded. CoDi is prohibitively expensive to train and therefore excluded. Continuous (cont.) and categorical (cat.) features are indicated on the axes.

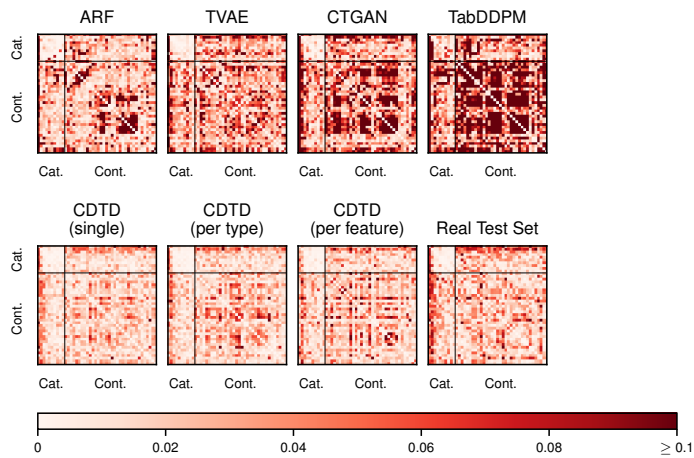


Figure 20: Element-wise absolute differences of the correlation matrices between the real training set and the synthetic data for the lending dataset. CoDi is prohibitively expensive to train and therefore excluded. Continuous (cont.) and categorical (cat.) features are indicated on the axes.

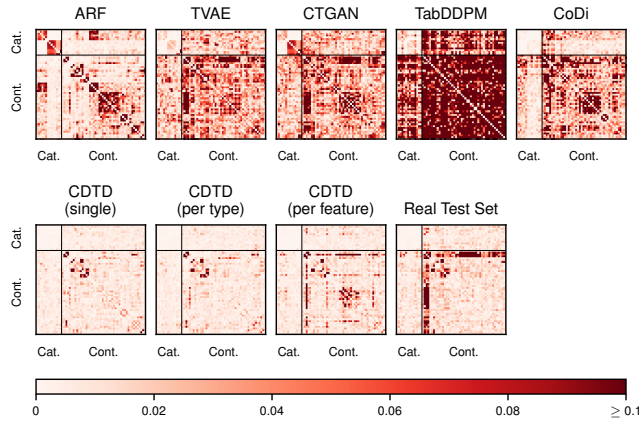


Figure 21: Element-wise absolute differences of the correlation matrices between the real training set and the synthetic data for the news dataset. Continuous (cont.) and categorical (cat.) features are indicated on the axes.

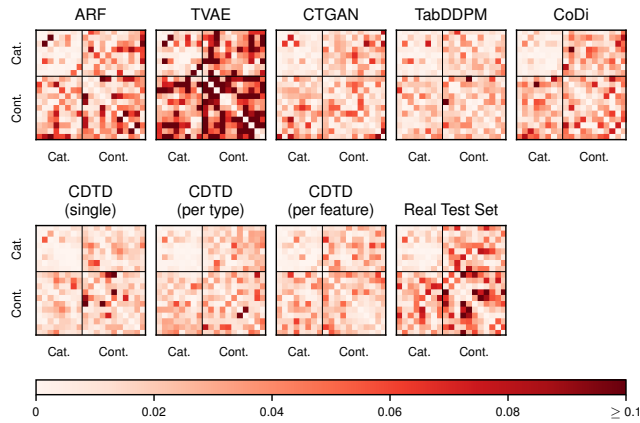


Figure 22: Element-wise absolute differences of the correlation matrices between the real training set and the synthetic data for the nmes dataset. Continuous (cont.) and categorical (cat.) features are indicated on the axes.

## N Detailed Results

CoDi is prohibitively expensive to train on `lending` and `diabetes` and TabDDPM produces NaNs for `acsincome` and `diabetes`. For both models, the performance metrics on these datasets are therefore not reported.

Table 6: Model evaluation results averaged over 11 datasets (skipping a dataset if the model was not trainable on it) for five benchmark models and for CDTD with three different noise schedules. Per performance metric, **bold** indicates the best, underline the second best result.

	ARF	CTGAN	TVAE	TabDDPM	CoDi	CDTD (single)	CDTD (per type)	CDTD (per feature)
RMSE (abs. diff.; ↓)	0.094	0.674	0.947	0.486	0.173	<b>0.084</b>	0.101	0.110
FI (abs. diff.; ↓)	0.053	0.130	0.074	<b>0.015</b>	0.044	0.025	<u>0.020</u>	0.025
AUC (abs. diff.; ↓)	0.020	0.080	0.065	<b>0.009</b>	0.027	0.018	<u>0.016</u>	0.022
L <sub>2</sub> distance of corr. (↓)	1.321	2.187	2.745	3.786	1.200	<u>0.782</u>	<b>0.756</b>	0.990
Detection score (↓)	0.934	0.986	0.976	<u>0.769</u>	0.936	0.796	<b>0.768</b>	0.783
JSD (↓)	<b>0.011</b>	0.114	0.152	0.051	0.038	<u>0.015</u>	0.016	0.018
WD (↓)	0.011	0.023	0.025	0.061	0.022	0.010	<b>0.007</b>	<u>0.009</u>
DCR (abs. diff. to test; ↓)	1.588	3.336	1.621	<b>0.568</b>	1.000	0.796	0.806	<u>0.758</u>

Table 7: L<sub>2</sub> norm (incl. standard errors in subscripts) of the correlation matrix differences of real and synthetic train sets for five benchmark models and for CDTD with three different noise schedules.

	ARF	CTGAN	TVAE	TabDDPM	CoDi	CDTD (single)	CDTD (per type)	CDTD (per feature)
<code>acsincome</code>	0.242±0.002	1.696±0.008	1.136±0.004	-	0.517±0.006	0.141±0.003	0.129±0.003	0.119±0.002
<code>adult</code>	0.576±0.006	1.858±0.010	0.735±0.012	0.156±0.006	0.493±0.009	0.170±0.007	0.125±0.009	0.128±0.010
<code>bank</code>	0.819±0.024	0.947±0.019	2.758±0.049	0.898±0.025	0.499±0.021	0.323±0.008	0.266±0.011	0.256±0.015
<code>beijing</code>	0.133±0.006	1.445±0.009	1.642±0.015	1.133±0.035	0.363±0.015	0.075±0.008	0.073±0.009	0.071±0.004
<code>churn</code>	0.635±0.026	1.355±0.043	1.301±0.041	0.327±0.044	0.746±0.062	0.302±0.041	0.289±0.043	0.282±0.044
<code>covertime</code>	1.192±0.017	3.685±0.005	4.668±0.003	1.044±0.001	1.029±0.032	2.359±0.011	2.275±0.009	2.710±0.009
<code>default</code>	1.228±0.021	2.697±0.021	1.564±0.029	3.408±0.105	1.672±0.061	0.627±0.068	0.652±0.102	0.737±0.033
<code>diabetes</code>	1.189±0.004	1.654±0.008	5.351±0.095	-	-	1.201±0.020	0.803±0.032	1.345±0.016
<code>lending</code>	3.473±0.057	2.420±0.016	5.895±0.026	10.675±0.015	-	1.042±0.075	1.189±0.040	1.363±0.097
<code>news</code>	4.333±0.128	4.641±0.028	4.612±0.016	15.985±0.081	4.874±0.148	1.925±0.527	2.035±0.475	3.395±0.950
<code>nmes</code>	0.717±0.054	1.663±0.035	0.532±0.030	0.447±0.031	0.609±0.032	0.433±0.025	0.478±0.083	0.481±0.058

Table 8: Jensen-Shannon divergence (incl. standard errors in subscripts) for five benchmark models and for CDTD with three different noise schedules.

	ARF	CTGAN	TVAE	TabDDPM	CoDi	CDTD (single)	CDTD (per type)	CDTD (per feature)
<code>acsincome</code>	0.013±0.001	0.256±0.000	0.309±0.000	-	0.076±0.001	0.025±0.001	0.024±0.000	0.022±0.001
<code>adult</code>	0.007±0.001	0.112±0.001	0.113±0.001	0.034±0.001	0.045±0.001	0.010±0.001	0.013±0.001	0.016±0.000
<code>bank</code>	0.004±0.000	0.086±0.001	0.191±0.001	0.029±0.001	0.038±0.001	0.010±0.000	0.009±0.001	0.012±0.001
<code>beijing</code>	0.005±0.002	0.147±0.003	0.257±0.001	0.035±0.003	0.018±0.004	0.003±0.001	0.005±0.002	0.005±0.001
<code>churn</code>	0.011±0.004	0.095±0.003	0.048±0.004	0.014±0.004	0.043±0.001	0.012±0.003	0.012±0.002	0.011±0.002
<code>covertime</code>	0.002±0.000	0.044±0.000	0.043±0.000	0.004±0.000	0.008±0.000	0.008±0.000	0.008±0.000	0.011±0.000
<code>default</code>	0.008±0.001	0.194±0.001	0.177±0.001	0.027±0.002	0.073±0.002	0.013±0.001	0.015±0.001	0.015±0.001
<code>diabetes</code>	0.009±0.000	0.093±0.000	0.187±0.000	-	-	0.022±0.000	0.023±0.000	0.026±0.000
<code>lending</code>	0.049±0.002	0.092±0.001	0.188±0.001	0.243±0.002	-	0.055±0.001	0.056±0.001	0.064±0.002
<code>news</code>	0.002±0.001	0.022±0.001	0.128±0.001	0.046±0.000	0.012±0.001	0.003±0.001	0.003±0.001	0.003±0.001
<code>nmes</code>	0.008±0.002	0.117±0.002	0.029±0.003	0.028±0.004	0.027±0.003	0.008±0.001	0.009±0.001	0.013±0.003

Table 9: Wasserstein distance (incl. standard errors in subscripts) for five benchmark models and for CDTD with three different noise schedules.

	ARF	CTGAN	TVAE	TabDDPM	CoDi	CDTD (single)	CDTD (per type)	CDTD (per feature)
<code>acsincome</code>	0.007±0.000	0.037±0.000	0.021±0.000	-	0.017±0.000	0.002±0.000	0.001±0.000	0.001±0.000
<code>adult</code>	0.012±0.000	0.016±0.000	0.021±0.000	0.003±0.000	0.013±0.000	0.006±0.000	0.004±0.000	0.003±0.000
<code>bank</code>	0.012±0.000	0.021±0.000	0.040±0.001	0.011±0.000	0.030±0.001	0.006±0.001	0.004±0.000	0.004±0.000
<code>beijing</code>	0.009±0.000	0.021±0.000	0.058±0.001	0.011±0.000	0.019±0.000	0.004±0.000	0.003±0.000	0.002±0.000
<code>churn</code>	0.013±0.001	0.027±0.001	0.032±0.001	0.008±0.002	0.048±0.002	0.008±0.001	0.007±0.001	0.006±0.001
<code>covertime</code>	0.006±0.000	0.041±0.000	0.022±0.000	0.003±0.000	0.012±0.000	0.017±0.000	0.015±0.000	0.012±0.000
<code>default</code>	0.005±0.000	0.011±0.000	0.009±0.000	0.005±0.000	0.013±0.000	0.004±0.000	0.004±0.000	0.003±0.000
<code>diabetes</code>	0.012±0.000	0.020±0.000	0.038±0.000	-	-	0.038±0.000	0.020±0.000	0.042±0.000
<code>lending</code>	0.013±0.001	0.011±0.000	0.016±0.000	0.425±0.001	-	0.009±0.000	0.010±0.000	0.011±0.000
<code>news</code>	0.024±0.000	0.009±0.000	0.018±0.000	0.078±0.001	0.030±0.000	0.007±0.000	0.006±0.000	0.008±0.000
<code>nmes</code>	0.012±0.000	0.036±0.000	0.008±0.000	0.007±0.001	0.016±0.001	0.006±0.001	0.006±0.001	0.006±0.000

Table 10: Detection score (incl. standard errors in subscripts) for five benchmark models and for CDTD with three different noise schedules.

	ARF	CTGAN	TVAE	TabDDPDM	CoDi	CDTD (single)	CDTD (per type)	CDTD (per feature)
accincome	0.808 $\pm$ 0.001	0.989 $\pm$ 0.001	0.985 $\pm$ 0.000	-	0.825 $\pm$ 0.002	0.540 $\pm$ 0.003	0.532 $\pm$ 0.004	0.526 $\pm$ 0.002
adult	0.889 $\pm$ 0.002	0.997 $\pm$ 0.000	0.967 $\pm$ 0.001	0.590 $\pm$ 0.003	0.992 $\pm$ 0.001	0.604 $\pm$ 0.002	0.588 $\pm$ 0.002	0.591 $\pm$ 0.005
bank	0.955 $\pm$ 0.002	1.000 $\pm$ 0.000	0.988 $\pm$ 0.001	0.783 $\pm$ 0.003	1.000 $\pm$ 0.000	0.795 $\pm$ 0.003	0.739 $\pm$ 0.003	0.694 $\pm$ 0.006
beijing	0.995 $\pm$ 0.000	0.998 $\pm$ 0.000	0.993 $\pm$ 0.001	0.966 $\pm$ 0.002	0.997 $\pm$ 0.001	0.951 $\pm$ 0.002	0.949 $\pm$ 0.001	0.947 $\pm$ 0.002
churn	0.853 $\pm$ 0.002	0.945 $\pm$ 0.006	0.843 $\pm$ 0.011	0.561 $\pm$ 0.005	0.730 $\pm$ 0.012	0.621 $\pm$ 0.016	0.533 $\pm$ 0.007	0.544 $\pm$ 0.031
covertime	0.945 $\pm$ 0.002	0.997 $\pm$ 0.000	0.989 $\pm$ 0.001	0.586 $\pm$ 0.002	0.900 $\pm$ 0.002	0.991 $\pm$ 0.001	0.992 $\pm$ 0.001	0.991 $\pm$ 0.001
default	0.991 $\pm$ 0.001	0.998 $\pm$ 0.001	0.997 $\pm$ 0.001	0.821 $\pm$ 0.002	0.995 $\pm$ 0.000	0.827 $\pm$ 0.004	0.802 $\pm$ 0.003	0.871 $\pm$ 0.001
diabetes	0.854 $\pm$ 0.002	0.935 $\pm$ 0.002	0.997 $\pm$ 0.001	-	-	0.858 $\pm$ 0.001	0.780 $\pm$ 0.002	0.866 $\pm$ 0.002
lending	0.997 $\pm$ 0.001	0.995 $\pm$ 0.002	0.995 $\pm$ 0.001	1.000 $\pm$ 0.000	-	0.955 $\pm$ 0.006	0.954 $\pm$ 0.009	0.961 $\pm$ 0.004
news	0.998 $\pm$ 0.000	1.000 $\pm$ 0.000	1.000 $\pm$ 0.000	0.966 $\pm$ 0.002	1.000 $\pm$ 0.000	0.973 $\pm$ 0.001	0.953 $\pm$ 0.001	0.977 $\pm$ 0.001
nmes	0.987 $\pm$ 0.002	0.992 $\pm$ 0.003	0.988 $\pm$ 0.002	0.650 $\pm$ 0.014	0.988 $\pm$ 0.000	0.636 $\pm$ 0.008	0.623 $\pm$ 0.008	0.642 $\pm$ 0.010

Table 11: Distance to closest record of the generated data (incl. standard errors in subscripts) for five benchmark models and for CDTD with three different noise schedules.

	ARF	CTGAN	TVAE	TabDDPDM	CoDi	CDTD (single)	CDTD (per type)	CDTD (per feature)
accincome	8.637 $\pm$ 0.027	10.758 $\pm$ 0.054	6.652 $\pm$ 0.032	-	10.877 $\pm$ 0.092	8.346 $\pm$ 0.056	8.322 $\pm$ 0.047	8.349 $\pm$ 0.033
adult	2.523 $\pm$ 0.012	5.012 $\pm$ 0.028	2.227 $\pm$ 0.013	1.647 $\pm$ 0.009	2.735 $\pm$ 0.028	1.112 $\pm$ 0.019	1.231 $\pm$ 0.011	1.294 $\pm$ 0.009
bank	3.025 $\pm$ 0.017	3.840 $\pm$ 0.014	3.136 $\pm$ 0.007	2.327 $\pm$ 0.010	3.062 $\pm$ 0.012	1.828 $\pm$ 0.008	1.943 $\pm$ 0.007	2.062 $\pm$ 0.008
beijing	0.735 $\pm$ 0.003	1.004 $\pm$ 0.006	0.926 $\pm$ 0.003	0.739 $\pm$ 0.006	0.610 $\pm$ 0.002	0.490 $\pm$ 0.002	0.489 $\pm$ 0.001	0.477 $\pm$ 0.002
churn	1.136 $\pm$ 0.015	1.804 $\pm$ 0.036	1.146 $\pm$ 0.039	0.342 $\pm$ 0.031	0.852 $\pm$ 0.016	0.332 $\pm$ 0.021	0.274 $\pm$ 0.021	0.276 $\pm$ 0.012
covertime	1.741 $\pm$ 0.011	5.773 $\pm$ 0.017	3.173 $\pm$ 0.013	0.889 $\pm$ 0.007	1.508 $\pm$ 0.020	2.297 $\pm$ 0.026	2.209 $\pm$ 0.022	2.252 $\pm$ 0.013
default	3.095 $\pm$ 0.026	5.880 $\pm$ 0.020	3.216 $\pm$ 0.013	1.422 $\pm$ 0.013	2.593 $\pm$ 0.020	1.127 $\pm$ 0.028	1.269 $\pm$ 0.014	1.253 $\pm$ 0.012
diabetes	17.736 $\pm$ 0.107	21.935 $\pm$ 0.046	8.214 $\pm$ 0.022	-	-	15.279 $\pm$ 0.026	15.126 $\pm$ 0.058	15.350 $\pm$ 0.059
lending	17.776 $\pm$ 0.132	20.239 $\pm$ 0.222	10.688 $\pm$ 0.025	12.537 $\pm$ 0.076	-	13.775 $\pm$ 0.147	14.162 $\pm$ 0.188	13.960 $\pm$ 0.282
news	6.147 $\pm$ 0.010	4.789 $\pm$ 0.005	5.821 $\pm$ 0.003	4.960 $\pm$ 0.006	4.661 $\pm$ 0.023	3.635 $\pm$ 0.004	3.687 $\pm$ 0.006	3.749 $\pm$ 0.048
nmes	2.203 $\pm$ 0.028	2.971 $\pm$ 0.008	1.710 $\pm$ 0.019	0.891 $\pm$ 0.033	1.231 $\pm$ 0.024	0.664 $\pm$ 0.029	0.710 $\pm$ 0.032	0.771 $\pm$ 0.023

Table 12: Machine learning efficiency F1 score for five benchmark models, the real training data and for CDTD with three different noise schedules. The standard deviation takes into account five different sampling seeds and uses the average results of the four machine learning efficiency models computed across ten model seeds.

	Real Data	ARF	CTGAN	TVAE	TabDDPDM	CoDi	CDTD (single)	CDTD (per type)	CDTD (per feature)
adult	0.797 $\pm$ 0.000	0.769 $\pm$ 0.002	0.647 $\pm$ 0.015	0.756 $\pm$ 0.002	0.787 $\pm$ 0.001	0.745 $\pm$ 0.004	0.787 $\pm$ 0.001	0.787 $\pm$ 0.001	0.787 $\pm$ 0.001
bank	0.745 $\pm$ 0.002	0.682 $\pm$ 0.006	0.680 $\pm$ 0.006	0.629 $\pm$ 0.006	0.720 $\pm$ 0.006	0.673 $\pm$ 0.006	0.776 $\pm$ 0.003	0.767 $\pm$ 0.004	0.737 $\pm$ 0.004
churn	0.873 $\pm$ 0.003	0.780 $\pm$ 0.015	0.761 $\pm$ 0.009	0.802 $\pm$ 0.017	0.857 $\pm$ 0.007	0.865 $\pm$ 0.008	0.854 $\pm$ 0.011	0.852 $\pm$ 0.006	0.845 $\pm$ 0.011
covertime	0.817 $\pm$ 0.001	0.783 $\pm$ 0.001	0.442 $\pm$ 0.008	0.711 $\pm$ 0.002	0.799 $\pm$ 0.001	0.767 $\pm$ 0.001	0.734 $\pm$ 0.002	0.754 $\pm$ 0.002	0.722 $\pm$ 0.002
default	0.674 $\pm$ 0.001	0.627 $\pm$ 0.003	0.686 $\pm$ 0.002	0.632 $\pm$ 0.007	0.678 $\pm$ 0.002	0.638 $\pm$ 0.008	0.670 $\pm$ 0.002	0.671 $\pm$ 0.001	0.673 $\pm$ 0.003
diabetes	0.621 $\pm$ 0.002	0.572 $\pm$ 0.005	0.557 $\pm$ 0.004	0.553 $\pm$ 0.003	-	-	0.617 $\pm$ 0.002	0.617 $\pm$ 0.002	0.611 $\pm$ 0.002

Table 13: Machine learning efficiency AUC score for five benchmark models, the real training data and for CDTD with three different noise schedules. The standard deviation takes into account five different sampling seeds and uses the average results of the four machine learning efficiency models computed across ten model seeds.

	Real Data	ARF	CTGAN	TVAE	TabDDPDM	CoDi	CDTD (single)	CDTD (per type)	CDTD (per feature)
adult	0.915 $\pm$ 0.000	0.901 $\pm$ 0.000	0.836 $\pm$ 0.006	0.889 $\pm$ 0.002	0.908 $\pm$ 0.000	0.880 $\pm$ 0.005	0.910 $\pm$ 0.000	0.910 $\pm$ 0.001	0.909 $\pm$ 0.000
bank	0.947 $\pm$ 0.000	0.938 $\pm$ 0.001	0.934 $\pm$ 0.003	0.830 $\pm$ 0.020	0.940 $\pm$ 0.005	0.929 $\pm$ 0.005	0.945 $\pm$ 0.000	0.945 $\pm$ 0.001	0.943 $\pm$ 0.004
churn	0.964 $\pm$ 0.001	0.939 $\pm$ 0.007	0.882 $\pm$ 0.006	0.948 $\pm$ 0.004	0.957 $\pm$ 0.004	0.961 $\pm$ 0.001	0.962 $\pm$ 0.001	0.962 $\pm$ 0.001	0.959 $\pm$ 0.003
covertime	0.892 $\pm$ 0.000	0.860 $\pm$ 0.001	0.677 $\pm$ 0.007	0.777 $\pm$ 0.001	0.876 $\pm$ 0.000	0.845 $\pm$ 0.001	0.816 $\pm$ 0.002	0.828 $\pm$ 0.001	0.802 $\pm$ 0.002
default	0.768 $\pm$ 0.000	0.754 $\pm$ 0.002	0.744 $\pm$ 0.002	0.751 $\pm$ 0.004	0.763 $\pm$ 0.002	0.739 $\pm$ 0.008	0.762 $\pm$ 0.003	0.765 $\pm$ 0.002	0.765 $\pm$ 0.002
diabetes	0.693 $\pm$ 0.001	0.669 $\pm$ 0.002	0.626 $\pm$ 0.003	0.592 $\pm$ 0.002	-	-	0.675 $\pm$ 0.001	0.673 $\pm$ 0.001	0.667 $\pm$ 0.001

Table 14: Machine learning efficiency RMSE for five benchmark models, the real training data and for CDTD with three different noise schedules. The standard deviation takes into account five different sampling seeds and uses the average results of the four machine learning efficiency models computed across ten model seeds.

	Real Data	ARF	CTGAN	TVAE	TabDDPDM	CoDi	CDTD (single)	CDTD (per type)	CDTD (per feature)
accincome	0.804 $\pm$ 0.012	0.757 $\pm$ 0.007	2.292 $\pm$ 0.013	1.054 $\pm$ 0.011	-	0.857 $\pm$ 0.010	0.838 $\pm$ 0.015	0.811 $\pm$ 0.014	0.820 $\pm$ 0.011
beijing	0.712 $\pm$ 0.001	0.792 $\pm$ 0.007	1.246 $\pm$ 0.010	1.690 $\pm$ 0.016	0.606 $\pm$ 0.006	0.912 $\pm$ 0.005	0.774 $\pm$ 0.005	0.770 $\pm$ 0.005	0.762 $\pm$ 0.005
lending	0.030 $\pm$ 0.000	0.274 $\pm$ 0.007	0.137 $\pm$ 0.007	0.404 $\pm$ 0.007	0.795 $\pm$ 0.031	-	0.061 $\pm$ 0.001	0.060 $\pm$ 0.001	0.066 $\pm$ 0.002
news	1.001 $\pm$ 0.002	0.923 $\pm$ 0.052	1.906 $\pm$ 0.019	3.999 $\pm$ 0.175	0.083 $\pm$ 0.001	1.302 $\pm$ 0.074	0.819 $\pm$ 0.103	0.755 $\pm$ 0.091	0.755 $\pm$ 0.066
nmes	1.001 $\pm$ 0.003	0.972 $\pm$ 0.024	1.331 $\pm$ 0.052	1.127 $\pm$ 0.047	1.154 $\pm$ 0.047	1.137 $\pm$ 0.052	1.108 $\pm$ 0.083	1.184 $\pm$ 0.076	1.203 $\pm$ 0.081

## O Ablation Study Details

Table 15:  $L_2$  norm (incl. standard errors in subscripts) of the correlation matrix differences of real and synthetic train sets for five CDTD configurations with progressive addition of model components.

Configuration	A	B	C	D	CDTD (per type)
acsincome	$0.131_{\pm 0.003}$	$0.119_{\pm 0.004}$	$0.124_{\pm 0.006}$	$0.129_{\pm 0.004}$	$0.129_{\pm 0.003}$
adult	$0.131_{\pm 0.007}$	$0.128_{\pm 0.008}$	$0.168_{\pm 0.017}$	$0.107_{\pm 0.011}$	$0.125_{\pm 0.009}$
beijing	$0.065_{\pm 0.009}$	$0.066_{\pm 0.012}$	$0.067_{\pm 0.011}$	$0.067_{\pm 0.010}$	$0.073_{\pm 0.009}$
churn	$0.244_{\pm 0.015}$	$0.272_{\pm 0.034}$	$0.299_{\pm 0.066}$	$0.264_{\pm 0.012}$	$0.289_{\pm 0.043}$

Table 16: Jensen-Shannon divergence (incl. standard errors in subscripts) for five CDTD configurations with progressive addition of model components.

Configuration	A	B	C	D	CDTD (per type)
acsincome	$0.025_{\pm 0.000}$	$0.025_{\pm 0.001}$	$0.025_{\pm 0.001}$	$0.024_{\pm 0.001}$	$0.024_{\pm 0.000}$
adult	$0.012_{\pm 0.001}$	$0.013_{\pm 0.000}$	$0.012_{\pm 0.000}$	$0.014_{\pm 0.001}$	$0.013_{\pm 0.001}$
beijing	$0.004_{\pm 0.001}$	$0.006_{\pm 0.002}$	$0.005_{\pm 0.003}$	$0.004_{\pm 0.002}$	$0.005_{\pm 0.002}$
churn	$0.010_{\pm 0.002}$	$0.008_{\pm 0.002}$	$0.009_{\pm 0.004}$	$0.010_{\pm 0.002}$	$0.012_{\pm 0.002}$

Table 17: Wasserstein distance (incl. standard errors in subscripts) for five CDTD configurations with progressive addition of model components.

Configuration	A	B	C	D	CDTD (per type)
acsincome	$0.002_{\pm 0.000}$	$0.002_{\pm 0.000}$	$0.002_{\pm 0.000}$	$0.001_{\pm 0.000}$	$0.001_{\pm 0.000}$
adult	$0.004_{\pm 0.000}$	$0.005_{\pm 0.000}$	$0.006_{\pm 0.000}$	$0.003_{\pm 0.000}$	$0.004_{\pm 0.000}$
beijing	$0.003_{\pm 0.000}$	$0.004_{\pm 0.000}$	$0.003_{\pm 0.000}$	$0.003_{\pm 0.000}$	$0.003_{\pm 0.000}$
churn	$0.006_{\pm 0.001}$	$0.006_{\pm 0.000}$	$0.006_{\pm 0.001}$	$0.006_{\pm 0.001}$	$0.007_{\pm 0.001}$

Table 18: Detection score (incl. standard errors in subscripts) for five CDTD configurations with progressive addition of model components.

Configuration	A	B	C	D	CDTD (per type)
acsincome	$0.534_{\pm 0.002}$	$0.534_{\pm 0.001}$	$0.538_{\pm 0.003}$	$0.532_{\pm 0.002}$	$0.532_{\pm 0.004}$
adult	$0.597_{\pm 0.002}$	$0.593_{\pm 0.001}$	$0.615_{\pm 0.003}$	$0.580_{\pm 0.003}$	$0.588_{\pm 0.002}$
beijing	$0.953_{\pm 0.002}$	$0.959_{\pm 0.001}$	$0.952_{\pm 0.003}$	$0.953_{\pm 0.001}$	$0.949_{\pm 0.001}$
churn	$0.557_{\pm 0.014}$	$0.573_{\pm 0.014}$	$0.564_{\pm 0.012}$	$0.541_{\pm 0.015}$	$0.533_{\pm 0.007}$

Table 19: Distance to closest record of the generated data (incl. standard errors in subscripts) for five CDTD configurations with progressive addition of model components.

	Real Test Set	A	B	C	D	CDTD (per type)
acsincome	$7.673_{\pm 0.017}$	$8.335_{\pm 0.064}$	$8.222_{\pm 0.035}$	$8.305_{\pm 0.021}$	$8.352_{\pm 0.025}$	$8.322_{\pm 0.047}$
adult	$1.870_{\pm 0.000}$	$1.221_{\pm 0.018}$	$1.294_{\pm 0.015}$	$1.252_{\pm 0.014}$	$1.427_{\pm 0.008}$	$1.231_{\pm 0.011}$
beijing	$0.385_{\pm 0.000}$	$0.545_{\pm 0.001}$	$0.559_{\pm 0.002}$	$0.539_{\pm 0.003}$	$0.541_{\pm 0.002}$	$0.489_{\pm 0.001}$
churn	$0.347_{\pm 0.000}$	$0.307_{\pm 0.016}$	$0.326_{\pm 0.009}$	$0.294_{\pm 0.022}$	$0.298_{\pm 0.013}$	$0.274_{\pm 0.021}$

Table 20: Machine learning efficiency F1 score for five CDTD configurations with progressive addition of model components. The standard deviation accounts for five different sampling seeds and uses the average results of the four machine learning efficiency models across ten model seeds.

	<b>Real Data</b>	<b>A</b>	<b>B</b>	<b>C</b>	<b>D</b>	<b>CDTD (per type)</b>
<b>adult</b>	0.797 $\pm$ 0.000	0.788 $\pm$ 0.001	0.788 $\pm$ 0.001	0.787 $\pm$ 0.001	0.788 $\pm$ 0.002	0.787 $\pm$ 0.001
<b>churn</b>	0.873 $\pm$ 0.003	0.856 $\pm$ 0.008	0.856 $\pm$ 0.014	0.857 $\pm$ 0.007	0.849 $\pm$ 0.006	0.852 $\pm$ 0.006

Table 21: Machine learning efficiency AUC score for five CDTD configurations with progressive addition of model components. The standard deviation accounts for five different sampling seeds and uses the average results of the four machine learning efficiency models across ten model seeds.

	<b>Real Data</b>	<b>A</b>	<b>B</b>	<b>C</b>	<b>D</b>	<b>CDTD (per type)</b>
<b>adult</b>	0.915 $\pm$ 0.000	0.909 $\pm$ 0.000	0.910 $\pm$ 0.000	0.909 $\pm$ 0.000	0.910 $\pm$ 0.000	0.910 $\pm$ 0.001
<b>churn</b>	0.964 $\pm$ 0.001	0.962 $\pm$ 0.002	0.961 $\pm$ 0.003	0.960 $\pm$ 0.002	0.961 $\pm$ 0.001	0.962 $\pm$ 0.001

Table 22: Machine learning efficiency RMSE for five CDTD configurations with progressive addition of model components. The standard deviation accounts for five different sampling seeds and uses the average results of the four machine learning efficiency models across ten model seeds.

	<b>Real Data</b>	<b>A</b>	<b>B</b>	<b>C</b>	<b>D</b>	<b>CDTD (per type)</b>
<b>accincome</b>	0.804 $\pm$ 0.012	0.815 $\pm$ 0.009	0.813 $\pm$ 0.018	0.823 $\pm$ 0.017	0.814 $\pm$ 0.014	0.811 $\pm$ 0.014
<b>beijing</b>	0.712 $\pm$ 0.001	0.782 $\pm$ 0.004	0.785 $\pm$ 0.004	0.778 $\pm$ 0.005	0.776 $\pm$ 0.004	0.770 $\pm$ 0.005



## P Training and Sampling Times Details

Table 23: Training times in minutes. TabDDPM produces NaNs during training on acsincome and diabetes, and is therefore excluded for these data. CoDi is considered prohibitively expensive to train on diabetes and lending and we report estimated (est.) training times.

	ARF	CTGAN	TVAE	TabDDPM	CoDi	CTD (per feature)
acsincome	80.3	59.9	26.0	-	231.9	5.8
adult	7.4	36.2	23.7	38.3	48.3	6.9
bank	11.0	37.6	24.6	40.5	42.7	26.3
beijing	3.7	34.3	23.9	36.1	24.9	23.4
churn	0.3	27.1	13.7	18.2	25.7	6.1
covertime	130.2	58.0	36.5	44.9	69.2	28.2
default	12.0	38.3	24.8	38.9	45.9	26.4
diabetes	58.5	90.1	25.3	-	870 (est.)	26.9
lending	5.2	157.9	36.6	48.7	3000 (est.)	25.3
news	23.0	48.8	33.3	37.2	41.5	25.2
nmes	0.4	32.8	17.2	24.9	30.2	6.3

Table 24: Sample times in seconds per 1000 samples.

	ARF	CTGAN	TVAE	TabDDPM	CoDi	CTD (per feature)
acsincome	4.20	0.23	0.07	-	10.26	0.59
adult	1.78	0.31	0.16	0.82	3.65	0.56
bank	2.24	0.44	0.44	0.87	3.38	0.64
beijing	0.34	0.41	0.32	2.09	2.45	0.26
churn	1.00	0.40	0.24	0.95	2.78	0.39
covertime	9.74	0.28	0.25	2.45	4.35	1.97
default	2.07	0.27	0.25	0.86	3.48	0.60
diabetes	5.87	0.53	0.15	-	-	1.33
lending	2.49	0.45	0.54	4.33	-	0.69
news	3.89	0.43	0.30	5.13	2.93	0.85
nmes	1.54	0.31	0.17	4.17	2.91	0.55